Bachelor thesis by
Jakob Jersild Nielsen
August 2019

Characterisation of fibrotic transcriptional signatures in mouse adipose tissue using RNA-Seq

Karakterisering af fibrotiske transcriptionelle signaturer i muse adipøst væv ved brug af RNA-Seq

Number of characters including spaces: 76225

Supervised by
Professor Susanne Mandrup
PhD student Elvira Laila Van Hauwaert

Contents

Acknowledgements

I would like to express my very great appreciation to Professor Susanne Mandrup for the opportunity of conducting this project in her laboratory in addition to her advice and assitance with the project. I would like to offer my special thanks to PhD student Elvira Laila Van Hauwaert for her valuable guidance and supervision in the progress of this project. Additionally, I wish her all the best with her maternity. My grateful thanks are also extended to Tenna Pavia Mortensen and technicians of the laboratory for their patience and assitance with operating in the laboratory. Lastly, I would like to thank the remaining Mandrup group for their kindness and openness.

Abstract

In modern society overfeeding is common. Overfeeding often results in overweight and obesity, which in turn can cause various metabolic complications and comorbidities. One of the consequences of obesity can be adipose tissue fibrosis, which interferes with the organ functionality.

In this project, the transcriptomic changes of the epididymal white adipose tissue (eWAT) and inguinal white adipose tissue (iWAT) in male CL57BL/6J mice have been characterised during the early stages of diet-induced obesity-associated fibrosis development. The characterisation was accomplished using RNA sequencing (RNA-Seq), where the data were subjected to various analyses including differential expression analyses, hierarchical clustering and pathway analyses along with integrated motif activity response analyses (ISMARA). The eWAT expansion happened through hypertrophy, resulting in the tissue being hypoxic and inflamed along with progressively developing fibrosis. The iWAT was expanding through both hyperplasia and hypertrophy, causing the tissue to be hypoxic and only marginally inflamed. Development of early fibrosis was not observed in the iWAT. Lastly, a list of 61 transcription factors were identified that might be important drivers of early fibrosis development in eWAT.

Resume

I moderne samfund er overspisning almindeligt. Overspisning fører ofte til overvægt og fedme, som til gengæld kan forårsage forskellige metaboliske komplikationer og komorbiditeter. En af konsekvenserne af fedme kan være udvikling af fibrose i de adipøse væv, hvilket interfererer med vævsfunktionaliteten.

I dette projekt karakteriseres de transkriptomiske forandringer i det epididymale hvide fedtvæv (eWAT) og det inguinale hvide fedtvæv (iWAT) i han CL57BL/6J mus under de tidlige stadier af diætinduceret fedme-associeret fibrose. Karakteriseringen blev opnået ved brug af RNA-sekvensering (RNA-Seq), hvor dataene undergik forskellige analyser, herunder differentiel ekspressionsanalyser, hierarkiske grupperingsanalyser, pathway analyser samt integrerede motivaktivitet responsanalyser (ISMARA). Det viste sig at eWAT ekspanderede gennem hypertrofi, hvilket resulterede i hypoxia, inflammation og begyndende fibroseudvikling. Desuden viste det sig, at iWAT ekspanderede gennem både hypertrofi og hyperplasi, hvilket resulterede i hypoxia og marginal vævsinflammation. Der blev ikke påvist begyndende udvikling af fibrose i iWAT. Afslutningsvist blev der identificeret 61 potentielle transskriptionsfaktorer, der kunne have en betydning for udviklingen af fibrose i eWAT.

Introduction

Since 1980, the prevalence of obesity and overweight have doubled (1). It is estimated that nearly half of the world's population is overweight, and a third is obese (1, 2). The overall health-care treatment costs of obese individuals in the US were increased by 14.3 percentage from 2005 to 2010 (3). Thus, obesity does not only constitute a significant health risk by increasing the risk of developing various comorbidities (1, 4-9) but likewise burdens the economics of society (2).

Measures of obesity

The most common measure of obesity is body mass index (BMI), although measures such as waist circumference (WC) and waist to hip circumference ratio (WHR) appear more useful regarding abdominal obesity (2). BMI is calculated as weight divided by height squared with weight in kilogram and height in meter. An individual with a BMI of 18.5-24.9 kg/m^2 is considered normal weighted, whereas an individual with a BMI of 25.0-29.9 kg/m^2 and 30.0-34.9 kg/m^2 is considered overweight and obese, respectively (2). Variations in adult BMIs are attributed to a combination of biological and environmental factors, with genetics and epigenetics accounting for approximately 70% (2).

Comorbidities of obesity

The cause of gaining weight is a result of that the energy intake exceeds the energy expenditure. If the positive energy balance becomes chronic, obesity may develop along with various metabolic conditions, commonly termed “metabolic syndrome” (10-12), and obesity-related comorbidities (2). The metabolic conditions of the metabolic syndrome are abdominal obesity, hypertension, low serum cholesterol levels and high-density lipoprotein (HDL), high serum TAG levels, and elevated fasting blood glucose levels (2). Metabolic syndrome is defined as a combination of at least three of the beforementioned metabolic conditions (2).

As mentioned initially, obesity constitutes a major health risk by increasing the risk of developing various comorbidities. One of the comorbidities is type 2 diabetes mellitus (T2DM) (2), considered to be the most significant comorbidity of obesity. There is controversy regarding the main cause of T2DM, one potential cause is free fatty acid (FFA)-induced oxidative stress promoted by reactive oxygen species production (2), whereas another is reductions in plasma adiponectin levels (13). Persisting T2DM is associated with additional complications, including cardiovascular diseases (CVD), peripheral vascular diseases (PVD), stroke, neuropathy, nephropathy and retinopathy (2, 14).

Long-term obesity is associated with exacerbation of cardiac function (15), ventricular mass enlargement (15), and potentially systolic dysfunction (16), atrial dilatation (16) and atrial fibrillation (17). An additional obesity-associated CVD is cardiomyopathy (18), which is characterised by diastolic dysfunction and hypertrophy of the left ventricle (18).

Another of the comorbidities of obesity is non-alcoholic fatty liver diseases (NAFLDs), which include hepatic steatosis, fibrosis, cirrhosis, and non-alcoholic steatohepatitis (2). Considerable attributes to NAFLDs are obesity and insulin resistance (2).

Kidney-comorbidities of obesity includes chronic kidney disease, abnormal renal parameters, obesity-related glomerulopathy, and increased albumin excretion rates (AER) (2).

Other obesity comorbidities are gastroesophageal reflux disease (2), cancers (2, 19), along with multiple airways and gonadal disorders (2). Airway disorders include obesity hypoventilation syndrome and obstructive sleep apnoea syndrome (2).

Adipocytes and adipose tissues

Every existing mammal has a variety of adipose tissues (AT); predominantly, these are white adipose tissues (WAT). WAT is further divided into subcutaneous WAT (SAT) and visceral WAT (VAT). Another type of adipose tissue that exists in most mammals is brown adipose tissues (BAT). White adipocytes and brown adipocytes are most abundant in WAT and BAT, respectively.

White adipocytes are specialised lipid storage facilitating cells that typically are characterised by their few mitochondria and a unilocular droplet, and origin from Pax7-/Myf5- stem cells (20) (Figure 1). Whenever there is a shortage of nutritional intake, triacylglycerols (TAGs) are released from the white adipocytes in response to organismal fasting (12, 21).

Brown adipocytes are quite different from white adipocytes, not only by having more abundant mitochondria; brown adipocytes origin from Pax7+/Myf5+ stem cells (20) (Figure 1). They can like white adipocytes store lipids but are unable to properly mobilise them in response to signalling induced by starvation (20). The brown adipocytes are, however, responsible for the thermogenic program. Through the action of uncoupling protein 1 (UCP1), brown adipocytes uncouple ATP synthase in their mitochondria, by facilitating a proton leakage in the inner mitochondrial membrane. By doing so, they convert the energy from the mitochondrial electrochemical gradient into thermal energy (20, 22, 23). UCP1 mediated thermogenesis is also referred to as non-shivering thermogenesis (23, 24).

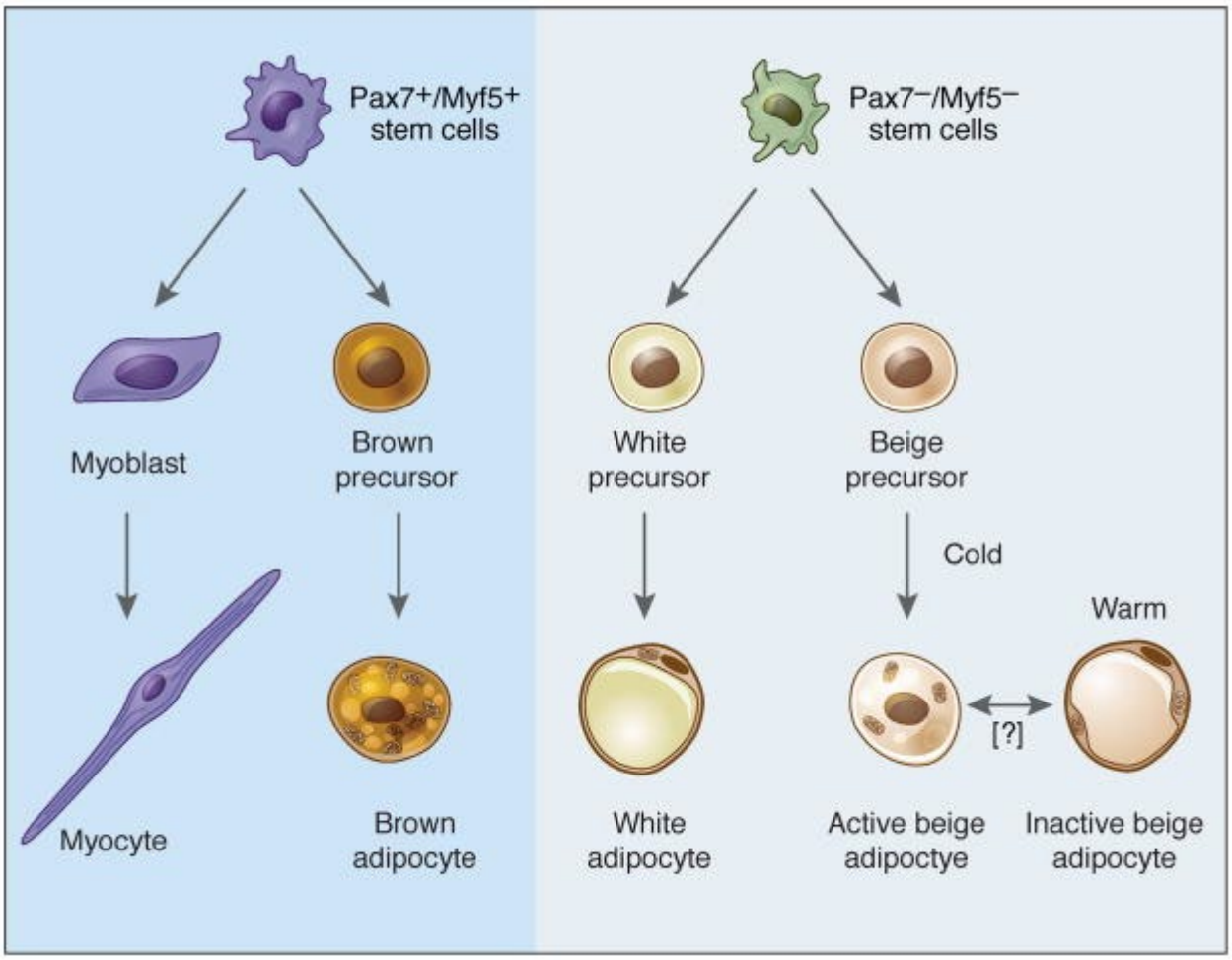

Figure 1. Origin of the different adipocytes. Brown adipocytes origin from Pax7+/Myf5+ stem cells, the same ancestor as myocytes, whereas white and beige adipocytes origin from Pax7-/Myf5- stem cells. Additionally, it is believed that white adipocytes can transdifferentiate into beige adipocytes. Figure from Rosen et al. 2014 (20).

The final type of adipocytes is beige adipocytes. Beige adipocytes and white adipocytes share mesenchymal stem cells as their ancestor, the Pax7-/Myf5- stem cells (20) (Figure 1). However, although they share the same ancestor, only the beige adipocytes can adopt both brown- and white-like phenotypes. They do so in response to cold and warmth exposure (23, 25), respectively.

In the modern era, the majority of *Homo sapiens* are insured regular meals, resulting in frequent nutritional intake, which exceeds the expenditure by the active metabolism (12, 26). When energy intake exceeds energy expenditure, the AT expands by enlargement of the exciting adipocytes by a process known as hypertrophy (12, 27, 28) or through another process known as hyperplasia (28, 29) (Figure 2). Hyperplasic adipose tissue expansion is characterised by an increase in the number of adipocytes through differentiation of adipose tissue-resident fibroblast-like preadipocytes into mature adipocytes (29). Hypertrophic adipose tissue

expansion is associated with increased free fatty acid release, pro-inflammatory cytokines, recruitment of immune cells along with hypoxia and fibrosis (28). Additionally, hypertrophic adipose tissues are associated with decreased adiponectin expression and impairments to the insulin sensitivity (28). Relative to hypertrophy, hyperplasia is associated with decreases in free fatty acid release, pro-inflammatory cytokines, recruitment of immune cells, hypoxia and fibrosis along with increases in adiponectin expression and amelioration of insulin sensitivity (28), whereas hyperplasic AT expansion is thought to be healthier than hypertrophic AT expansion (28).

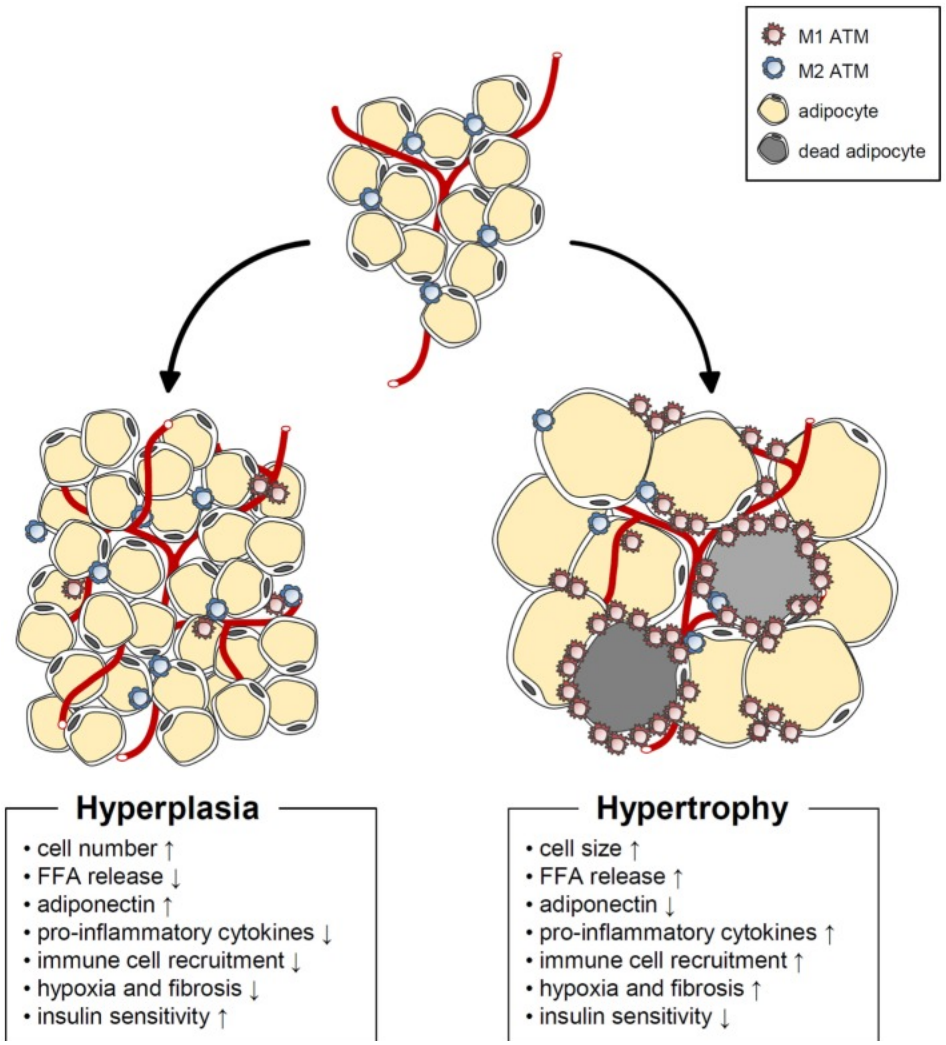

Figure 2. Characteristics of adipose tissue expansion through hypertrophy and hyperplasia. The adipose tissue can expand through two processes: hypertrophy and hyperplasia. Hypertrophic adipose tissue expansion happens through enlargement of current adipocytes and is associated with increased free fatty acid release, pro-inflammatory cytokines, recruitment of immune cells along with hypoxia and fibrosis. Additionally, hypertrophic adipose tissues are associated with decreased adiponectin expression and impairments to the insulin sensitivity. Hyperplasic adipose tissue expansion is characterised by an increase in number of adipocytes through differentiation of adipose tissue-resident fibroblast-like preadipocytes into mature adipocytes. Relative to hypertrophy, hyperplasia is associated with decreases in free fatty acid release, pro-inflammatory cytokines, recruitment of immune cells, hypoxia and fibrosis along with increases in adiponectin expression and amelioration of insulin sensitivity. Figure from Choe et al. 2016 (28).

Adipogenesis

Differentiation of preadipocytes into mature adipocytes are termed adipogenesis. In an *in vitro* model proposed by Siersbæk *et al.* 2012 (30), adipogenesis occurs through two waves of transcription factor (TF)-coordinated enhanceosome assembly (Figure 3). Enhanceosomes are enhancer-associated protein-complexes consisting of multiple TFs and cofactors collaborating to activate transcription successfully. In the model, key adipogenic TFs include the CCAAT-enhancer-binding protein (CEBP) family members CEBPα and CEBPβ, along with peroxisome proliferator-activated receptor gamma (PPARγ) (30, 31). CEBPβ binds to various genomic hotspots (30, 31), genomic regions occupied by multiple TFs (30), shortly after the initiation of adipogenesis, pioneering early enhanceosome assembly by modulating chromatin accessibility and facilitating recruitment of early adipogenic TFs (30, 32), including glucocorticoid receptor (GR), retinoid X receptor (RXR), Stat5a, CEBPδ (31, 33).

As the early adipogenic wave finalises, the late adipogenic wave is initiated. Many of the hotspots occupied by early adipogenic TFs are passed on to late adipogenic TFs. It has been suggested by Siersbæk *et al.* 2012 (30) that pioneering complexes in early adipogenesis containing CEBPβ remodel chromatin accessibility at PPARγ binding sites to subsequently assist with the bind of PPARγ (30-32). Furthermore, several early hotspots are located near the PPARγ gene, clearly underlining its importance (30). Aside from PPARγ, another important late adipogenic TF is CEBPα. Interestingly, most of the regulatory regions to which PPARγ binds are also bound by

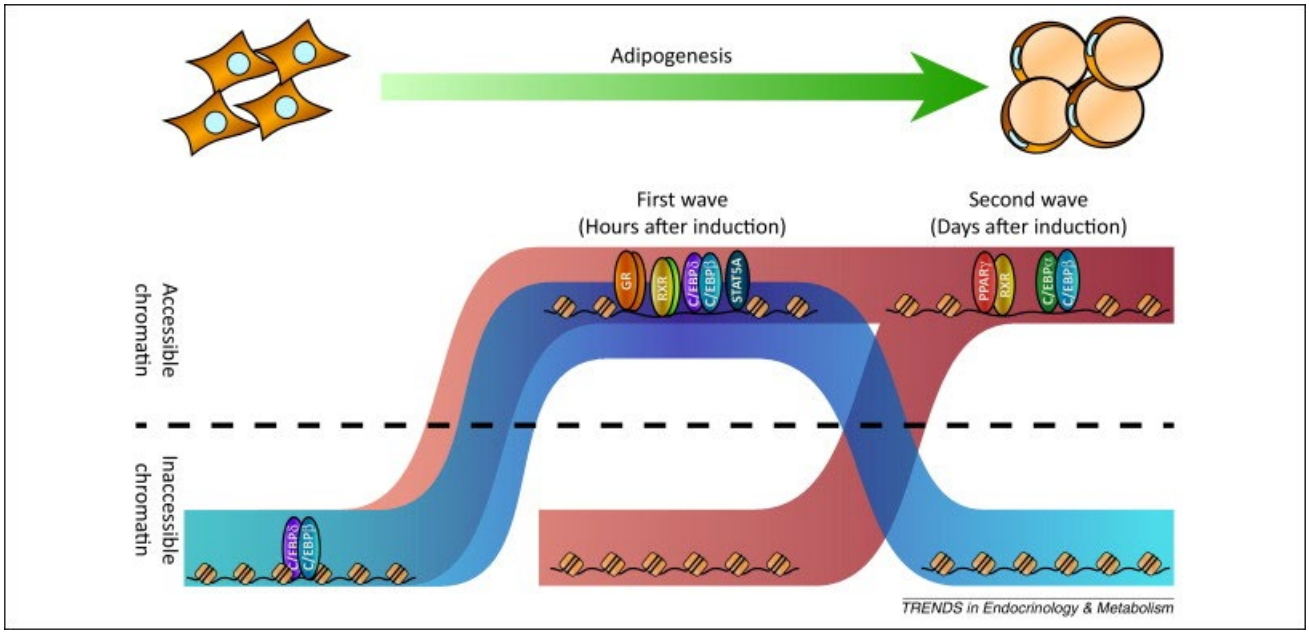

Figure 3. Illustration for the two adipogenic waves for transcription factor-mediated enhanceosome assembly. CEBPβ can interact with relative closed chromatin, whereas CEBPβ pioneers the early enhanceosome assembly by modulating chromatin accessibility. Figure from Lefterova et al. 2014 (31).

CEBPα (29). Together, PPARγ and CEBPα, act in synergy to finalise the second adipogenic wave and thus adipogenesis, producing fully mature adipocytes (29, 30).

Previously it was thought that whenever a precursor cell, e.g. a preadipocyte, differentiates into a mature cell, e.g. an adipocyte, it is entirely devoted to that lineage. However, recent studies suggest that adipocytes can de-differentiate into the fibroblast-like precursors and serve as precursors for entirely different cell lineages (34-38). An example of reversible de-differentiation of adipocytes is adipocytes in the mammary gland that de-differentiate into preadipocyte-like cells during pregnancy and lactation and re-differentiate back into adipocytes during involution of the mammary gland (37). Considering some cells can de-differentiate and re-differentiate into different cells, perhaps cell types should be defined from cellular plasticity.

Animal models of obesity

Considering the contemporary pandemic-scale health issue of obesity that humanity is facing, proper animal models of diet-induced obesity are required. Most commonly are small rodents used; these include mice, rats and marginally also hamsters. Mice and rats are frequently used when investigating diet-induced and age-related obesity (39). When deciding for an animal model, the essential goal is to find an animal with similar overall physiology and anatomy as *Homo sapiens* while being unambiguously breedable (39). Ideally, nonhuman primates can be used as they bear remarkable resemblances to *Homo sapiens*. Nonhuman primates have previously been used to study age-related obesity, diabetic and pre-diabetic treatments in clinical trials along with different metabolic disorders (40). Although nonhuman primate models can provide invulnerable insights into the details of certain aspects of obesity (40), mouse and rat models are still widely used within the field of research as they har easily genetically modified and provide results relatable to humans within a reasonable timeframe (39, 41, 42). Rodents are most commonly used for experimental purposes at an age-interval ranging between eight and twelve weeks (43). For academic institutions, the cost is a relatively high determining factor regarding the chosen age-interval (43), although they are not fully mature and still under development (44).

Adipose tissue state and adipocyte identity marker genes

Multiple genes specific to adipocytes and the AT can be used to verify both the identify and state of the adipose tissue. The expression of genes from processes such as lipid metabolism, uptake and transport are strong adipocyte identity marker genes. Examples of such genes are *fatty acid*

binding protein 4 (Fabp4), *lipoprotein lipase* (*Lpl)*, *perilipin 1 (Plin1)*, and *patatin-like phospholipase 1 (Pnpla1)*.

Fabp4 encodes the protein fatty acid binding protein 4 (FABP4), also known as adipocyte Protein 2 (AP2) (45). FABP family members can reversibly bind long-chain fatty acids, eicosanoids along with other lipids (45) and are proposedly involved in processes including lipid transport, lipid-mediated signalling, amongst others (45). Elevated serum levels of FABP4 are associated with obesity and a multiple of obesity-associated comorbidities (45).

Lpl encodes the protein lipoprotein lipase (LPL) that catalyses the hydrolysis of TAGs to non-esterified FFAs and 2-monoacylglycerol from chylomicrons and very low-density lipoproteins and is thus an indicator of adipocytic lipid uptake (46).

Plin1 encodes the protein perilipin 1 (PLIN1); a lipid-coated protein unique to adipocytes. PLIN1 is thought to be involved in both inflammation and homeostasis of lipid metabolism (47). In cows at least, low expression of PLIN1 is associated with increased lipid mobilisation and expression of pro-inflammatory cytokines through the nuclear factor kappa B (NFκB) pathway (47).

Pnpla1 encodes the protein adipose triglyceride lipase (ATGL) that is involved in intracellular TAG lipolysis together with hormone-sensitive lipase (HSL) and monoglyceride lipase (MGL) (48). ATGL is thus an indicator of adipocytic lipolytic activity.

Expression of genes encoding adipokines and AT-related TFs are strong indicators of the state of the AT and will be introduced below.

Adipokines

Cytokines secreted by adipocytes are termed adipokines, the first of which that was discovered was leptin in 1994 (49). Since 1994 hundreds of adipokines have been discovered, one of which is adiponectin (50).

Adiponectin, the gene product of *Adipoq*, is uniquely expressed by adipocytes in the AT and is secreted into the circulation, where it is involved in insulin sensitisation of some peripheral tissues, including the liver and muscles, by binding to its receptors, AdipoR1 and AdipoR2 (51-54). The signalling of AdipoR1 and AdipoR2 is mediated through activation of AMPK and PPARα (55), resulting in fatty acid oxidation, glucose uptake and lactate production (52, 56-59).

Leptin, the gene product of *Lep*, is involved in regulating energy homeostasis in the body by signalling through its receptor, obesity receptor b (ObRb); ObRb is mainly expressed in the hypothalamus (60), but is also, present on all types of immune cells (60). There is a total of six isoforms of the ObRs: ObRa-f (60). The isoform ObRb is the longest of the isoforms with the

greatest signal transduction capability (60). The isoform ObRe lacks intracellular domains, whereas it is secreted as a soluble receptor that can regulate serum concentrations of leptin (60). The remaining four receptor isoforms, ObRa, ObRc, ObRd and ObRf, are expressed on various cells, yet have less signal transduction capabilities relative to ObRb, as they contain fewer motifs necessary to activate their signal transduction pathway; ObRa is the most commonly expressed isoform (60). Leptin signalling is mainly mediated through the JAK/STAT signal transduction pathway (60). Secretion of leptin is regulated majorly by the amount of energy stored as lipids in ATs along with sudden changes in energy intake (61-66). Thus serum levels of leptin approximate the amount of fat stored in the ATs. Interestingly, decreases in leptin levels result in neuroendocrine mechanisms to counteract the change by increasing hunger and decreasing energy expenditure, amongst others, complicating cases of weight loss (64).

Adipose tissue-related transcription factors

Many TFs are involved in the regulation of processes of AT cells, some of which are mentioned below.

Members of the erythroblast transformation-specific (ETS) TF family are involved in a wide variety of biological and cellular processes including apoptosis, differentiation, proliferation, metastasis, migration, signalling pathways, amongst others (67). *ETS-related gene (Erg)* and *erythroblast transformation-specific 2 Ets2* are two of the genes encoding ETS TF family members. *Erg* encodes the TF ETS-related gene (ERG), whereas *Ets2* encodes erythroblast transformation-specific 2 (ETS2) (68). ETS TFs are defined by a highly conserved DNA-binding domain (DBD) termed the Ets domain (68). The ETS domain folds into a helix-turn-helix DNA-binding motif that binds to the DNA motif 5'-GGA(A/T)-3' (68). Most ETS TFs bind as a monomer to their genomic binding domain, where they are inhibited by flanking inhibiting DNA sequences (68). Enhancement of the ETS DBD activity and specificity is required to disinhibit ETS, which is achieved by kinase-mediated phosphorylation, amongst others (68). ETS TFs, including ETS2, has been shown to be functionally important for adipogenesis and possibly in regulating adipose tissue mass (69).

The gene product of *Hif1a* is the TF hypoxia-induced factor 1-alpha (HIF-1α) that is expressed in most cells and is under normal circumstances ubiquitinated (12, 70). This ubiquitination induces proteasome-mediated degradation of HIF-1α (12, 70). In normoxic (normal oxygen saturation) conditions, HIF-1α proline and asparaginyl residues are hydroxylated, leading to a highly increased affinity to a ubiquitin ligase complex, thus facilitating proteasome-mediated

degradation (12, 70). However, during hypoxia, e.g. in association with hypertrophic AT expansion (12, 27, 70), ubiquitination of HIF-1α is inhibited, as the proline and asparaginyl residues are not hydroxylated, resulting in reduced turnover of HIF-1α, and thus, increased abundance and activity (12, 70).

The TF family of NFκB includes the five structurally similar proteins: NFκB1, NFκB2, RelA, RelB and c-Rel (71). NFκB expression is amongst others induced by HIF-1α, leading to the expression of pro-inflammatory genes, encoding pro-inflammatory cytokines, chemokines, amongst others in hypoxia-associated hypertrophic AT (12, 27, 71). Transcription of NFκB target genes is mediated by binding of hetero- or dimerised NFκB to κB regulatory regions (71, 72). Usually, NFκB is sequestered in the cytoplasm by an inhibitor of kappa B (IκB) protein (71). Activation of NFκB can happen through either the canonical or noncanonical pathway, both important for regulation of immune and inflammatory responses (71). NFκB activation through the canonical pathway involves IκB kinase (IKK)-induced ubiquitin-dependent proteasome degradation of IκBα (71, 73). Contrarily, activation of NFκB through the noncanonical pathway involves NFκB inducing kinase (NIK)-induced processing of NFκB2 precursor to produce mature NFκB2 (71, 74, 75).

The transforming growth factor beta (TGFβ) superfamily consists of TGFβ, bone morphogenetic proteins (BMP), growth/differentiation factors (GDF), and activins, all of which control multiple processes in the AT including inflammation and adipogenesis (76). TGFβ itself is a cytokine that inhibits adipogenesis (76) and is involved in proliferation, differentiation and inflammation in a vast variety of cells and tissues (77-79) and is additionally considered to be pro-fibrotic (80). TGFβ family members signals through their receptors TβR1 and TβR2 (80), both of which exists as homodimers in the plasma membrane (81). When bound by ligand, the two receptor homodimers assembly into a complex, where TβR2 phosphorylates and activates TβR1, resulting in subsequent downstream signalling through the TGFβ/Smad signalling pathway (76, 80).

From high-fat diet exposure to adipose tissue fibrosis

Some of the processes involved in the progression of diet-induced obesity towards a more pathological state are hypoxia (70), inflammation (27, 82) and fibrosis (27, 83). These processes are described below.

Hypertrophic adipose tissue expansion-related hypoxia

Obese AT is typically associated with decreased local oxygen saturation, attributed to decreases in AT blood flow (84), leading to a hypoxic response (12, 27, 70). As mentioned earlier, during hypoxia, ubiquitination of HIF-1α is inhibited, as the proline and asparaginyl residues are not

hydroxylated, resulting in reduced turnover of HIF-1α and thus increased abundance. HIF-1α target genes include *vascular endothelial growth factor A (VEGFA*), which encodes vascular endothelial growth factor (VEGF); an angiogenic protein that stimulates angiogenesis (12, 70). The newly synthesised VEGF, induced by HIF-1α upregulation of *VEGFA*, acts as a mitogen in a paracrine manner on nearby vascular endothelial cells, thus stimulating angiogenesis (12, 85). Furthermore, adipogenesis is repressed under hypoxic conditions, where HIF-1α-regulated genes suppress PPARG2 expression (12, 86-88). It has also been shown that hypoxia induces necrosis and apoptosis in adipocytes (12, 89). Whenever an adipocyte, under hypoxic conditions, is unable to maintain the minimal requirement of ATP production, it becomes necrotic (12, 90). Necrosis could, in turn, induce pro-inflammatory M1 adipose tissue macrophages (ATM) recruitment through inflammation (12, 27, 88) along with transdifferentiation of anti-inflammatory M2 ATM into M1 ATM (12, 91). Additionally, hypoxia-induced expression of macrophage migration inhibition factor (MIF) in adipocytes and preadipocytes, inhibits macrophages from migrating away from the hypoxic tissue (88). M1 ATMs tend to surround necrotic adipocytes with a crown-like structure to collectively engulf them (12, 86) (Figure 2). HIF-1α also induces expression of NFκB in most cells of the AT (92), ultimately causing an inflammatory response, by further inducing the expression of pro-inflammatory genes, encoding pro-inflammatory cytokines, chemokines, amongst others (12, 27, 71).

Inflammatory immune cells in mouse adipose tissues

Although virtually every type of immune cell is present in the AT with varying phenotypes and proportions in lean and obese AT (93-97), macrophages are identified as being a major contributor to AT inflammation during DIO (95). Mediators of M1 ATM polarisation are adipokines, cytokines and chemokines secreted by adipocytes and immune cells (98, 99). M1 ATMs themselves secrete tumour necrosis factor alpha (TNF-α) and interleukin-6 (IL-6) that is associated with decreased systemic insulin sensitisation (95, 100) and further recruitment of M1 polarised ATMs, constituting a positive feedback loop (100). Adipocytes themselves have also been shown to secrete lower levels of TNFα, IL-6, and C-C motif chemokine ligand 2 (CCL2) (12, 101), whereas they induce M1 polarisation of macrophages (20). M1 polarised macrophages are predominantly abundant in obese adipose tissues, whereas M2 macrophages are dominating in the lean adipose tissues (20) (Figure 4).

In the early steps of AT inflammation, in visceral fat depots at least, T cells have been shown to have an essential function (102-105). T cells can be divided into two overall classes: CD8+ and

CD4+ T cells. CD8+ T cells are also termed cytotoxic T cells. CD4+ T cells can be divided further into T regulatory cells (Tregs) and T helper cells (Ths) (105). At least three Th subtypes have been discovered: Th1, Th2 and Th17. Th1 cells are induced by IL-12 and secrete the pro-inflammatory cytokine IFNγ, whereas Th2 cells are induced by IL-4 and secrete IL-4, IL-5, IL-10 and IL-13. Th17 cells are induced by both IL-6 and TGFβ and secrete IL-17 (105). IL12 is typically produced by antigen-presenting cells such as macrophages and dendritic cells (106). Additional subtypes that are believed to have a function regarding AT inflammation are Th9 and Th22 (105, 107, 108). Regarding DIO-related inflammation, the proportion of pro-inflammatory T cells such as CD4+ and CD8+ T is increased, whereas the proportion of anti-inflammatory T cells such as Tregs is decreased (105) (Figure 4).

B cells have been shown to be important in chronic inflammation. They can like T cells be divided into distinct subsets. These subsets are B1 and B2 cells (109, 110). B1 cells typically produce IgM antibody, although they can produce IgA in the gut (111, 112), whereas B2 cells produce antibodies to T dependent antigens (109). B2 cells can be divided further into subsets of mature

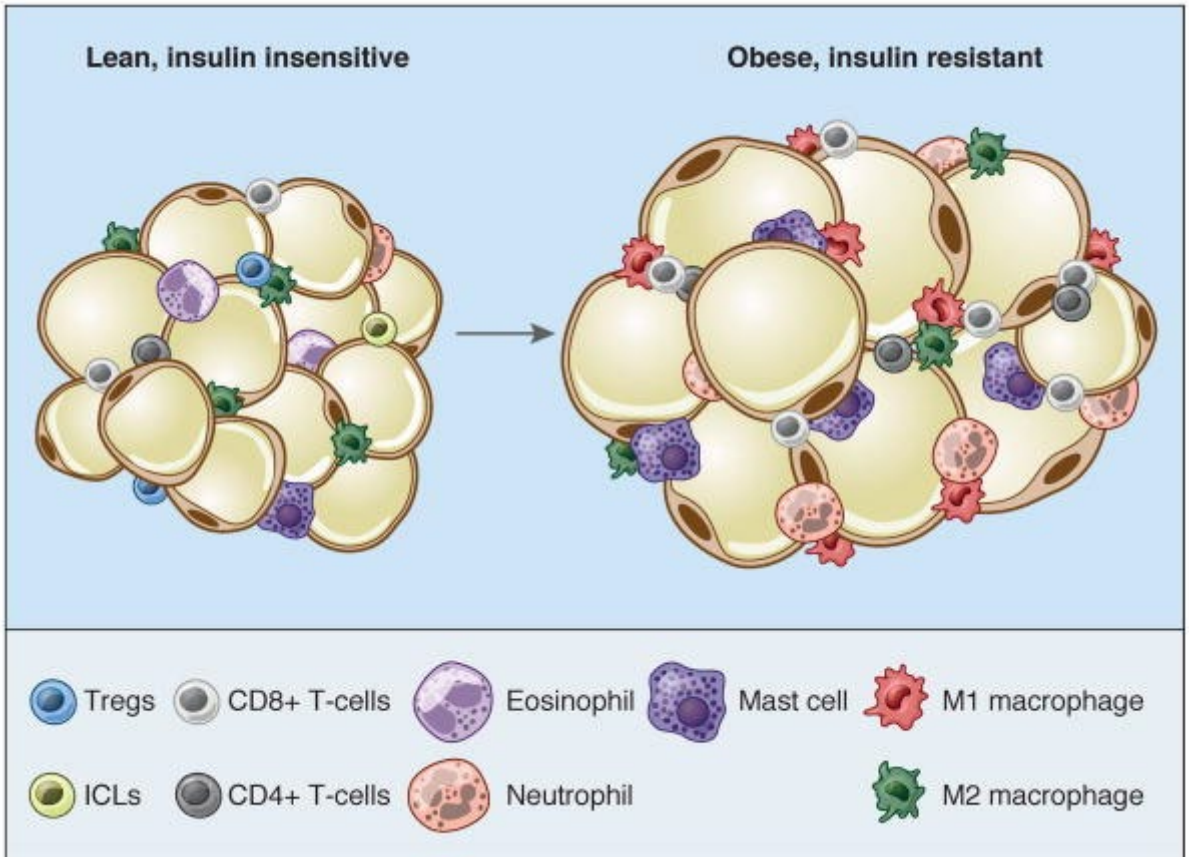

Figure 4. Proportions of immune cells in lean and obese adipose tissues. In lean adipose tissues the dominating immune cells are M2 polarised macrophages in addition to regulatory T cells and eosinophils. In obese adipose tissues the dominating immune cells are M1 polarised macrophages and mast cells, along with helper T cells (CD4+) and cytotoxic T cells (CD8+). Figure from Rosen et al. 2014 (20).

transitional and follicular B cells along with marginal zone B cells (109, 113). Like T cells, B2 cells are capable of producing a variety of cytokines, some of which are Th1-like and some that are Th2-like. The Th1-like cytokines include IFNγ, IL-12 and TNFα, whereas the Th2-like cytokines include IL-2, IL-4 and IL-13 (109). Additionally, some B cells produce the anti-inflammatory cytokine IL-10 (114, 115).

IFNγ, the secretory product of Th1 and some B2 cells, binds toll-like receptors (TLRs) on M1 ATMs, causing an increase in cytokine secretion, thus favouring chronic low-grade AT inflammation (100, 109, 116, 117) that eventually results in AT fibrosis (27, 96).

Diet-induced obesity-related fibrosis

Fibrosis is characterised by excessive extracellular matrix (ECM) deposition and is usually considered to be pathogenic, due to the reduction in organ functionality that typically associates with fibrosis (12, 118-121). New research does, however, question the definitive pathogenicity of AT fibrosis, suggesting both an adaptive and a maladaptive function of AT fibrosis (12, 83). The adaptive function of AT fibrosis is associated with an extensive shift in ECM composition in early obesity, where it stiffens and becomes less flexible, thereby limiting adipocyte hypertrophy. The hypertrophic limitation does, in turn, preserve adipocyte function (12, 83). Paradoxically, it also results in an ectopic fat deposition that could lead to amongst others, hepatic fibrosis (12, 122, 123). The maladaptive function of AT fibrosis is related to obesity-associated metabolic dysregulation where insulin-resistant subjects have been shown to have increased subcutaneous AT fibrosis relative to insulin-sensitive subjects (12, 83, 124).

The ECM is composed of a variety of structurally important protein, including collagens and adhesion proteins (125). Some of the AT adhesion proteins are fibronectin, elastins, laminin, along with proteoglycans such as decorin and perlecan (125). Collagens typically associated with fibrosis are type I, III and VI (125). Alterations in the ECM composition trigger integrin-mediated signalling pathways that are involved in cell-cell cohesion and regulation of a variety of processes including cell differentiation, proliferation, migration along with apoptosis and induction of gene transcriptions (125).

Other proteoglycans include matrix metalloproteinases (MMPs). MMPs regulate tissue architecture and are responsible for the degradation of ECM components such as collagens (125), thus the enzymatical activities partially determine the turnover of collagens. MMPs such as MMP-2 and MMP-9 can release TGFβ as a substrate-cleavage fragment from some ECM complexes, a previously introduced pro-fibrotic factor (125).

During obesity the transcriptional expression of some matricellular proteins is differentially expressed (125). Matricellular proteins are ECM proteins that do not contribute to the structure of the ECM, directly (126), but rather work indirectly by modulating cellular functions by interacting with structurally important ECM components such as collagens, along with cell-surface receptors, proteases and hormones (125, 126). The matricellular proteins include amongst others: osteopontins, secreted proteins acidic in nature-rich cysteine (SPARCs), thrombospondins (THBS) 1 and 2, along with Cyr61/CTGF/NOV (CCN) family members (125, 126). THBS1 is furthermore a regulator of TGFβ (125). Matricellular proteins might therefore be tremendously involved in progressive development of fibrosis by indirectly modulating the ECM composition, making them potential drug targets to hinder exacerbation of obesity-related comorbidities.

Aim of the study

This project aims to characterise the changes in the adipose tissue transcriptome during the early stages of adipose tissue fibrosis development in male mice during diet-induced obesity. These changes will be characterised in two major, but functionally different, white adipose tissues; the epididymal white adipose tissue (eWAT) and the inguinal white adipose tissue (iWAT).

Methods and Materials

Experimental setup

Male CL57BL/6J mice (Taconic Biosciences), with a starting age of 10 weeks, were fed either a high-fat diet (HFD) (Research Diets, #D12492) or a control low-fat diet (LFD) (Research Diets, #D12450B) for 12 weeks. Six mice from each group were sacrificed by cervical dislocation at week 0 (initiation of the experiment), week 6 and week 12, and inguinal white fat depots (iWAT) along with epididymal white fat depots (eWAT) was dissected and snap-frozen.

RNA extraction and purification

The adipose tissues, eWAT and iWAT, were isolated from the mice that were sacrificed by cervical dislocation, washed in PBS, followed by transferring them to Eppendorf tubes and snap freezing them in liquid nitrogen. The isolated tissues were homogenised in TRI Reagent (Sigma, TRI Reagent, T9424) using a FastPrep-24 5G Homogenizer (MP Biomedicals). The tissue lysates were transferred to new Eppendorf tubes on ice and added 0.2 volume chloroform (Sigma-Aldrich, Chloroform), vortexed for 30 seconds, then incubated for 15 minutes. Once finished incubating, the lysates were centrifuged at 10000rcf for 10 minutes at 4°C. The upper phase of

the lysates was transferred to new Eppendorf tubes on ice. There was added 0.6 volume of 96% vol. ethanol (GPR Rectapur, Ethanol 96 % vol) to the tubes, followed by a brief vortex and centrifugation. The contents of the tubes were loaded onto EconoSpin columns (Epoch Life Science, EconoSpin All-In-One Silica Mini Spin Columns) and centrifuged at 13000rcf for 30 seconds at RT. Afterwards, the columns were washed three times with RPE buffer, by centrifuging the columns at 13000rcf for 30 seconds at RT between each wash. The flowthrough of the columns was discarded. Once the last wash was completed, the columns were centrifuged dry at 13000rcf for 2 minutes at RT and were subsequently transferred to new Eppendorf tubes where they were incubated with open lids for 10 minutes at RT. To elute the RNA, a 30 µL drop of DEPC-treated water was placed onto the middle of the columns and incubated for 2 minutes at RT. After the incubation, the columns were centrifuged at 16000rcf for 1 minute at RT. The Eluted RNA was transferred to new Eppendorf tubes on ice, and the RNA concentration and quality were measured utilising a Spectrophotometer ND-1000 (NanoDrop) with 1µL of eluted RNA.

RNA integrity

To determine the RNA integrity of the samples, a 5300 Fragment Analyzer (Advanced Analytical) was used. Before preparing the samples, the FA was rinsed with 0.5M NaOH according to manufactures instructions in order to remove RNases. Samples with concentrations above the recommended maximum of 500µg/µL were diluted to achieve a concentration below the recommended maximum. The samples were loaded onto the first 11 columns' wells of a 96 deep well PCR plate (non-skirted plate) along with SS RNA diluent marker (Advanced Analytical). To the last columns' well of each row, SS RNA ladder (Advanced Analytical) along with SS RNA diluent marker was added. Additionally, a droplet of mineral oil was added to each of the used wells.

cDNA synthesis

Eppendorf tubes were placed on ice and added 1 µg RNA in DEPC-treated water to a total volume of 7µL, followed by 1µL DNase I (Invitrogen, 10U/µL DNase I) and 2µL DNase buffer (Invitrogen, 5X First Strand Buffer diluted 2:1 with DEPC-water). They were mixed by snapping the tubes and briefly centrifuged. Afterwards, the tubes were incubated for 15 minutes at 37°C. Once done incubating, the tubes were placed on ice and added 3 µg random hexamers, vortexed and centrifuged briefly. Next, the samples were incubated at 85°C for 5 minutes and placed on ice immediately after. Each of the samples was added a premix containing 5µL 5x1st Strand Buffer

(Invitrogen, 5X First Strand Buffer), 2.5µL dithiothreitol (Invitrogen, 0.1M DTT), 2.5µL deoxyribonucleotide triphosphate (MBI Fermentas, dNTP mix, 10mM each), 1µL Reverse Transcriptase (Invitrogen, M-MLV Reverse Transcriptase) and 1µL DEPC-treated water. The no Reverse Transcriptase samples were added additional DEPC-treated water instead of Reverse Transcriptase. After the addition of premix, they were incubated twice, once for 10 minutes at RT, and once for 1 hour at 37°C. Finally, the samples were added 200µL MilliQ water and stored at -80°C.

cDNA-qPCR

A 384 well plate (LightCycler 480 Multiwell Plate 384, white, Roche) was loaded with sample cDNA and MilliQ water in triplicates corresponding with a loading scheme prepared beforehand. After loading the plate with the samples, the plate was centrifuged at 1100rcf for 30 sec. To each of the wells, a mastermix containing FastStart Essential DNA Green Master (Roche), 5' primer, 3' primer and MilliQ water was added. Afterwards, the plate was centrifuged at 1100rcf for 30sec, wrapped in both LightCycler 480 sealing foil (Roche). The qPCR reactions where run on a LightCycler 480 Instrument II (Roche) under the following conditions: 2 min preincubation at 95°C and 45 cycles of 95°C for 15 sec; 60°C for 45 sec; 72°C for 45 sec. After the qPCR reactions, a melting curve was constructed by heating the samples from 60°C to 97°C.

RNA-Seq

Tubes were loaded with 1µg of sample RNA along with MilliQ water and handed off for prepping, where all the samples were prepped according to the manufacturer's instructions and subjected to paired-end sequencing on an Illumina NovaSeq 6000 sequencer. Subsequent data processing was performed in Unix and R.

Data processing

Initially, the data was processed in Unix using a script developed by Jesper Grud Skat Madsen[1] in order to conduct basal quality control of samples along with aligning the RNA-Seq data. The script utilises STAR (127) to align the RNA-Seq data, which generates BAM files. After the initial processing, quality control parameters were checked, and large files were downsampled to equal size randomisation using Samtools (128). Subsequently, gene read counting was performed using iRNA-Seq (129). In R, principal component analyses were performed on the RNA-Seq count data to determine if initial sample patterns can be established. Differential expression analyses

[1] Department of Biochemistry and Molecular Biology, University of Southern Denmark, Odense M 5230, Denmark.

were performed on the data output from iRNA-Seq using DESeq2 (130). The transcriptional levels of the selected genes were visualised in bar plots by normalising the gene counts to their transcript length and sequencing depth to transcripts per kilobase million (TPM). Hierarchical clustering and visualisation of clusters were performed on differentially expressed genes using pheatmap (131). Furthermore, pathway analyses were performed on the differentially expressed genes using clusterProfiler (132) and rWikiPathways (133). Integrated System for Motif Activity Response Analysis (ISMARA) (134) was used to identify potential TFs that could be important in regulating diet-induced obesity-related fibrosis.

Results And Discussion

High-fat diet induces weight gain in mice and their major adipose tissues

To characterise transcriptional changes in CL57BL/6J mice adipose tissues (AT) during diet-induced obesity (DIO)-related early development of AT fibrosis, mice were fed a high-fat diet (HFD) to induce weight gain. As a control, mice were fed a low-fat diet (LFD). Both groups of mice were weighed at different time points during the experiment; at week zero, five, six, eight, ten and twelve. These weights are plotted in a scatter plot together with their means (Figure 5A). The mice from the experiment fed with a HFD is seen to gradually increase their weight during the time course experiment relative to the mice fed with an LFD (Figure 5A). Although the HFD mice increase weight relative to the LFD mice, it is first at week eight and forwards that the weight of the HFD fed mice is significantly different from the weight of the LFD fed mice (Figure 5A). It is observable that the LFD fed mice gain weight relative to the week zero mice (Figure 5A), suggesting they are not fully developed at the time of the initiation of the experiment and thus are immature in terms of age.

At week zero, six and twelve, six mice from each dietary group were sacrificed and their epididymal white fat depots (eWAT) and inguinal white fat depots (iWAT) were dissected. To investigate whether diet the HFD caused weight gain at the tissue level as well, the tissues were weighed. The weights of the dissected eWAT and iWAT are plotted in a scatter plot together with their means (Figure 5B).

It is observable that there are weight increases from the week zero tissue dissections relative to the tissue dissections from the LFD fed mice at both time points after initiation of the experiment (Figure 5B). The developmental processes ongoing in CL57BL/6J mice at the age of ten weeks (age of the mice at the initiation of the experiment) include increase of bone mass along with

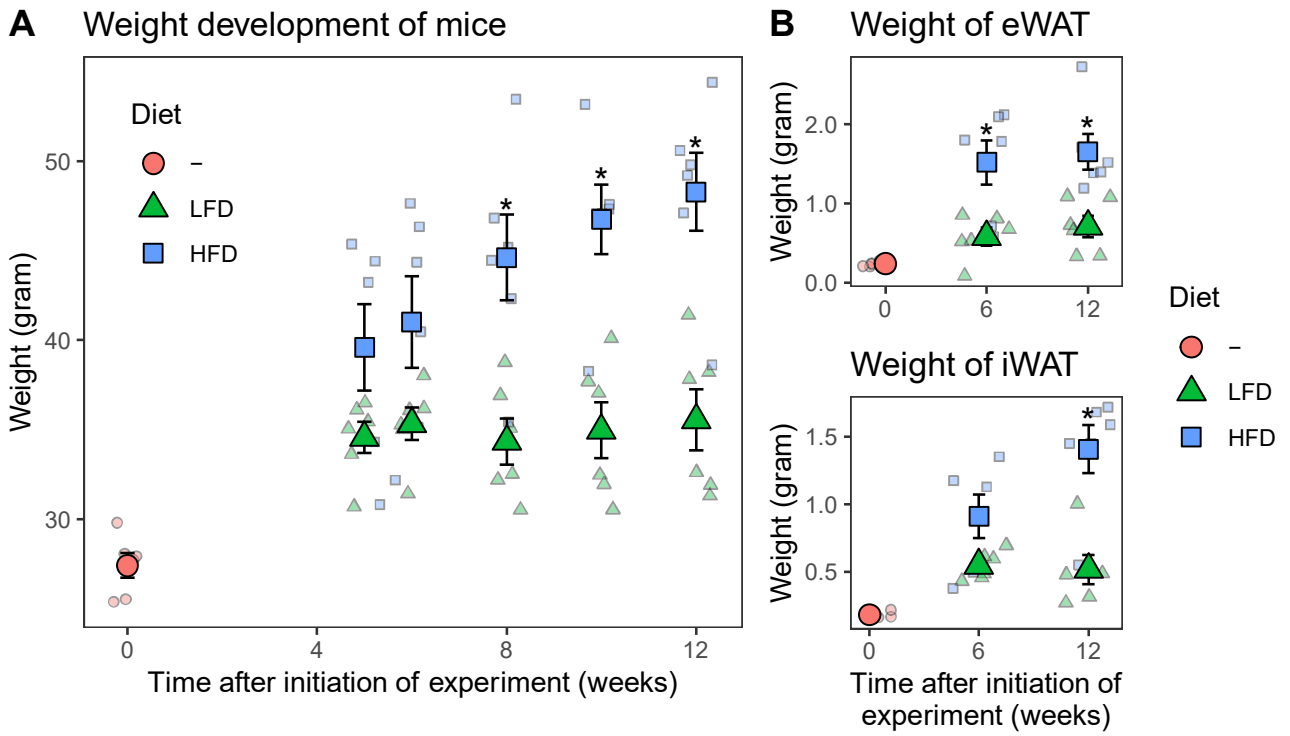

*Figure 5. Diet-induced weight changes of mice and their fat depots. (**A**) Data illustrating the weight development of the mice (n = 6) sacrificed at week 0, week 6 and week 12. Horizontally is the time after initiation of the experiment in weeks. Vertically is the weight of the mice in gram. Weights associated to mice from the week 0 group are coloured in red, whereas mice fed with a LFD or a HFD are coloured in green and blue, respectively. (**B**) Data illustrating the weight development of eWAT (upper) and iWAT (lower) of the mice (n = 6) sacrificed at week 0, week 6 and week 12. Horizontally is the time after initiation of the experiment in weeks. Vertically is the weight of the tissues in gram. Tissues from the week 0 group are coloured in red, whereas tissues from mice fed with a LFD or a HFD are coloured in green and blue, respectively. Transparent points (small) are the weights of individual mice plotted as jitters. All non-transparent points (large) are means of the weights. Error bars indicate standard error of mean. All * denotations indicate that the HFD mean is significantly different from the LFD mean at the indicated time point ($p < 0.05$). P values are calculated using a Student's t-test.*

development of the immune system and the nervous system (43). Specifically regarding the development of the nervous system, the mouse spinal cord, olfactory structures and hippocampus continuously develops until 11 weeks of age (43). Applying samples from the week zero mice as controls can thus potentially produce biased results when investigating diet-induced transcriptional changes, considering the ongoing developmental processes.

Interestingly, the age at which mice are commonly used for experimental purposes is from eight to twelve weeks (43), although many developmental processes are still ongoing, including increase of bone mass along with development of the immune system and the nervous system. A study published in Burlington Academic Press (44) defines CL57BL/6J mice as being mature from three to six months of age (44). Using mice with a starting age between three and six months in the experiment might therefore reduce transcriptional discrepancies attributed to

various developmental processes, and thus more clearly elucidate the diet-induced transcriptional changes of dietary exposure to a HFD or a LFD.

Tissue weights of eWAT and iWAT from the HFD group are increased in comparison to the LFD group (Figure 5B). The weight difference between eWAT of the HFD fed and LFD fed mice sacrificed at week six and twelve are shown to be significant, whereas only the weight difference between iWAT of the HFD fed and LFD fed mice sacrificed at week twelve are shown to be significant (Figure 5B). Comparing tissue weight gain of the dissected iWAT and eWAT depots, eWAT seems to have gained most weight at week six, with no or little weight gain from week six to twelve (Figure 5B, upper). In contrast, there could be a tendency of gradual weight gain during the time course experiment applying for iWAT, where the weight has increased from week six to twelve (Figure 5B, lower). It is known that the adipogenic potential, i.e. *de novo* differentiation of preadipocytes to adipocytes, of iWAT is greater compared to eWAT (135). With weight gain, iWAT depots expand by both hyperplasia and hypertrophy (136), whereas eWAT expands by hypertrophy exclusively (136). Thus, the significant changes in tissue weights at week 6 for eWAT might be a result of early tissue hypertrophy.

Less variance amongst eWAT replicates than iWAT replicates

In order to establish sample variance similarities before more extensive analyses, tissue-wise principal component analyses (PCA) are conducted on the RNA-Seq data (Figure 6).

It is observed that the eWAT tissue sample replicates (Figure 6A) cluster closer together than the iWAT tissue sample replicates (Figure 6B) and therefore have less variance between the replicates. Although, some discrepancies between replicates can be expected due to a combination of biological and technical variances, the overall variance within the iWAT dataset can lead to less significant discoveries when performing differential expression (DE) analyses.

The points representing the eWAT HFD samples are located to the right of the points representing the remaining samples (Figure 6A), indicating differences between the transcriptomes of the eWAT HFD samples relative to the eWAT week zero and eWAT LFD samples. Furthermore, the points representing the eWAT week twelve HFD samples seem to be shifted more to the right relative to the points representing the eWAT week six HFD samples (Figure 6A), indicating that there are more differences between the transcriptomes of the eWAT week twelve HFD samples than the eWAT week six HFD samples relative to the eWAT week zero and eWAT LFD samples. Considering there is extensive variance between the eWAT week zero

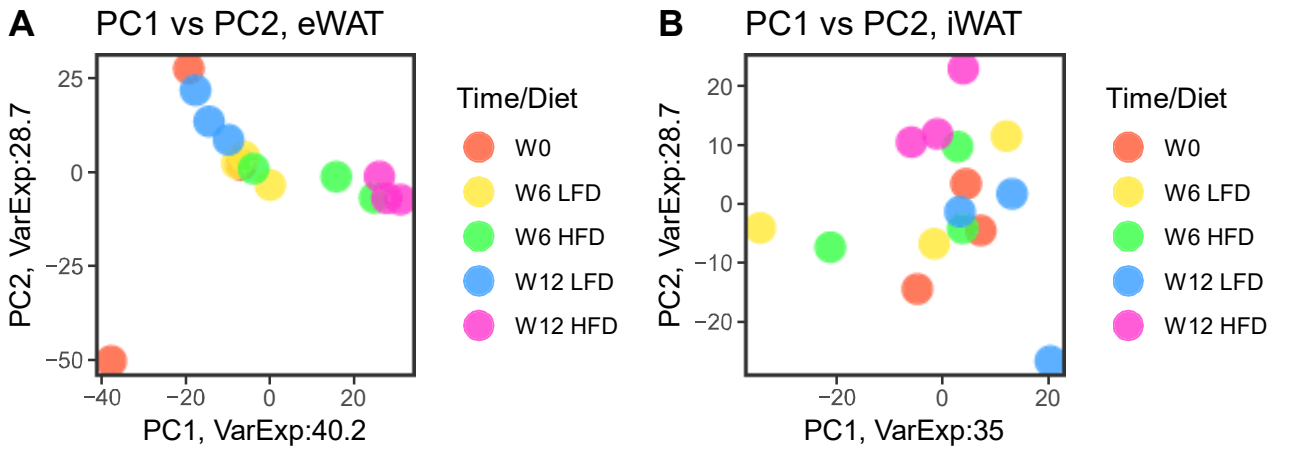

*Figure 6. Tissue-wise principal component analysis of RNA-Seq data. (**A**) PCA plot of eWAT samples. Horizontally is the first principal component (PC1) which explains 40.2% of the variance within the dataset. Vertically is the second principal component (PC2) which explains 28.7% of the variance within the dataset. (**B**) PCA plot of iWAT samples. Horizontally is the first principal component (PC1) which explains 35% of the variance within the dataset. Vertically is the second principal component (PC2) which explains 28.7% of the variance within the dataset. The points are coloured according to time of sacrifice and diet group.*

samples and as the points representing the eWAT LFD samples are located approximate to points representing the eWAT week zero samples (Figure 6A), no strong suggestions can be made regarding their transcriptomes. However, it seems that there is a slight top-left shift of the points representing the eWAT week twelve LFD samples relative to the points representing the eWAT week six LFD samples (Figure 6A).

No strong suggestions can be made regarding the iWAT samples considering the large variance between the replicates, although, there seem to be a marginal vertical shift of the points representing the iWAT week twelve HFD samples relative to the points representing the remaining samples (Figure 6B). The variance between the iWAT replicates is probably caused by the dissections. The iWAT is subcutaneous fat depot that is localised approximate to muscles, whereas iWAT dissections might contain some skin and muscle. Variable proportions of AT, skin and muscle can cause huge variances among replicates. Additional practice dissecting mouse ATs will potentially minimize replicate variances.

More significant transcriptional changes in eWAT than iWAT of LFD-fed mice

To investigate the transcriptional changes in male CL57BL/6J mouse AT attributed to early-life development and dietary change of chow-diet to LFD by performing tissue-wise DE analyses followed by hierarchical clustering of the differentially expressed genes and pathway analyses of the clusters of differentially expressed genes.

The tissue-wise DE analyses are conducted on combinations of the week zero and the week six and twelve LFD RNA-Seq data (Figure 7). Specifically, the following conditions were compared: eWAT week six LFD samples with eWAT week zero samples (Figure 7A); eWAT week twelve LFD samples with eWAT week zero samples (Figure 7B); eWAT week twelve LFD samples with eWAT week six LFD samples (Figure 7C); iWAT week six LFD samples with iWAT week zero samples (Figure 7D); iWAT week twelve LFD samples with iWAT week zero samples (Figure 7E); iWAT week twelve LFD samples with iWAT week six LFD samples (Figure 7F). Differentially expressed genes with LFCs greater than zero are upregulated in the first-mentioned conditions relative to the last-mentioned conditions, whereas differentially expressed genes with LFCs less than zero are downregulated in the first-mentioned conditions relative to the last-mentioned conditions. There are observed 2209 significant transcriptional differences between the eWAT week six LFD samples and the eWAT week zero samples, of which 648 genes are significantly upregulated and 1561 genes are significantly downregulated (Figure 7A); 1635 significant transcriptional

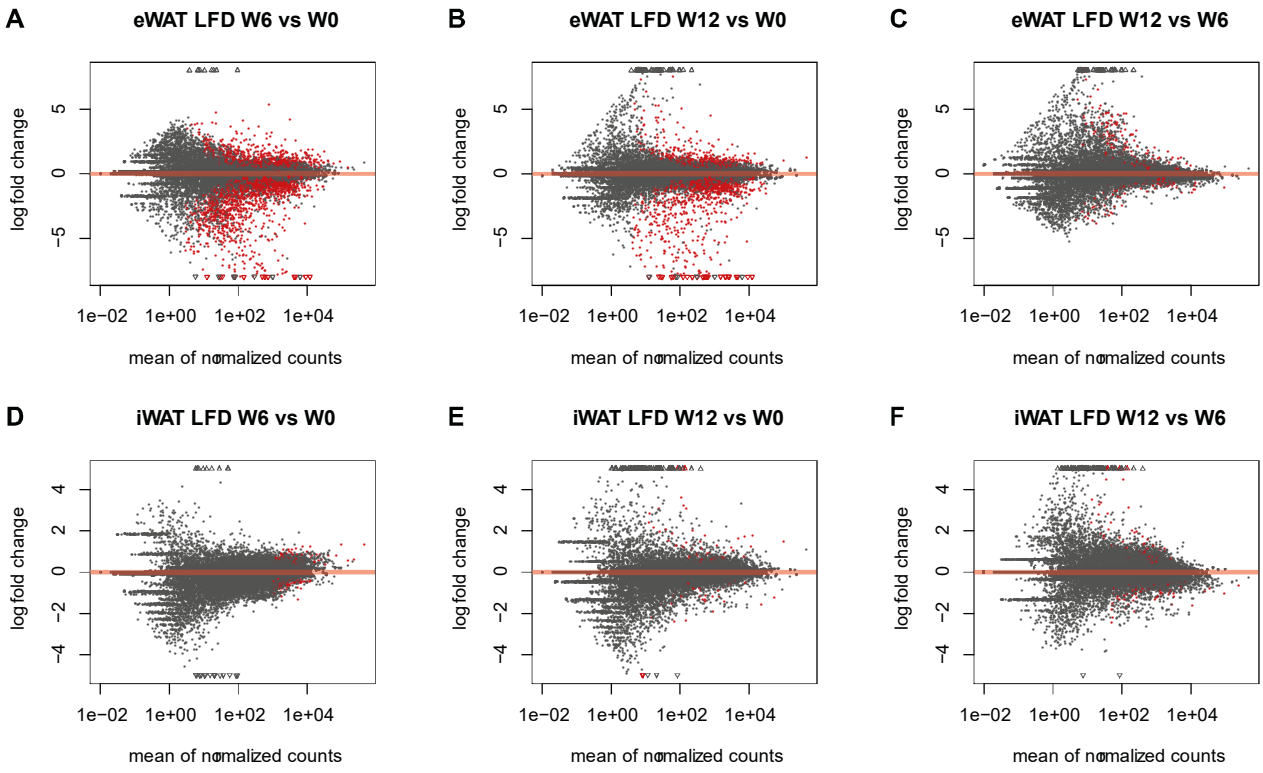

*Figure 7. Transcriptional changes of mouse adipose tissues in response to a low fat diet (LFD). Differential expression analyses of (**A**) eWAT week six LFD vs eWAT week zero samples, (**B**) eWAT week twelve LFD vs eWAT week zero samples, (**C**) eWAT week twelve vs eWAT week six LFD samples, (**D**) iWAT week six LFD vs iWAT week zero samples, (**E**) iWAT week twelve LFD vs iWAT week zero samples, and (**F**) iWAT week twelve vs iWAT week six LFD samples. Vertically is the log2 fold change. Horisontally is the mean of the normalised counts. Significant (FDR > 0.05) and non-significant differentially expressed genes are coloured in red and grey, respectively. P-values are corrected for multiple testing by the Benjamini-Hochberg procedure.*

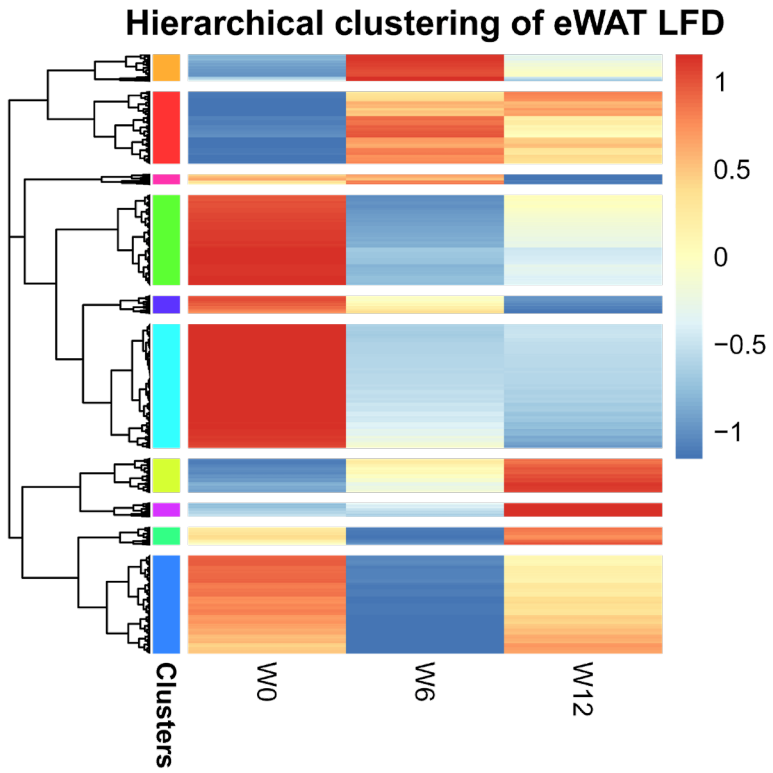

Figure 8. Hierarchical clustering of significant differentially expressed genes identified through differential expression analyses on eWAT LFD and week zero samples. The significant differentially expressed genes are divided into ten clusters. The clusters have been appointed appropriate colours according to the visible light spectrum (red, orange, yellow, lime green, spring green, cyan, dodger blue, dark blue, orchid purple and deep pink). The genes are coloured according to TPM values that are scaled by row.

differences are observed between the eWAT week twelve LFD samples and the eWAT week zero samples, of which 412 genes are significantly upregulated and 1223 genes are significantly downregulated (Figure 7B); 193 significant transcriptional differences are observed between the eWAT week twelve LFD samples and the eWAT week six LFD samples, of which 92 genes are significantly upregulated and 101 genes are significantly downregulated (Figure 7C); 23 significant transcriptional differences are observed between the eWAT week twelve LFD samples and the eWAT week six LFD samples, of which 12 genes are significantly upregulated and 11 genes are significantly downregulated (Figure 7D); 81 significant transcriptional differences are observed between the eWAT week twelve LFD samples and the eWAT week six LFD samples, of which 50 genes are significantly upregulated and 31 genes are significantly downregulated (Figure 7E); 80 significant transcriptional differences are observed between the eWAT week twelve LFD samples and the eWAT week six LFD samples, of which 45 genes are significantly upregulated and 35 genes are significantly downregulated (Figure 7F).

In total, between the mentioned eWAT conditions, there are 3030 unique significant differentially expressed genes, of which 878 of the genes are significantly upregulated and 2152

of the genes are significantly downregulated (Figure 7A-C). For the mentioned iWAT conditions, 160 of the significant differentially expressed genes are unique, of which 88 of the genes are significantly upregulated and 72 of the genes are significantly downregulated (Figure 7D-F).
The low amount of significant differentially expressed genes for the iWAT conditions are explained by the variance between the replicates (Figure 6B).
In order to investigate which biological processes the gene products of the significant differentially expressed genes across the time course experiment are related to, a pathway analysis was performed. First, the significantly regulated genes were clustered according to similar expression patterns, and then each cluster was subjected to pathway analysis. This allows for identification of biological processes that can be attributed to down- or upregulated genes across the time course experiment. Considering only a few significant differentially expressed genes were identified for the iWAT LFD and week zero samples, hierarchical clustering will only be performed on the significant differentially expressed genes identified for the eWAT LFD and week zero samples (Figure 8). The pathway analysis of the eWAT LFD

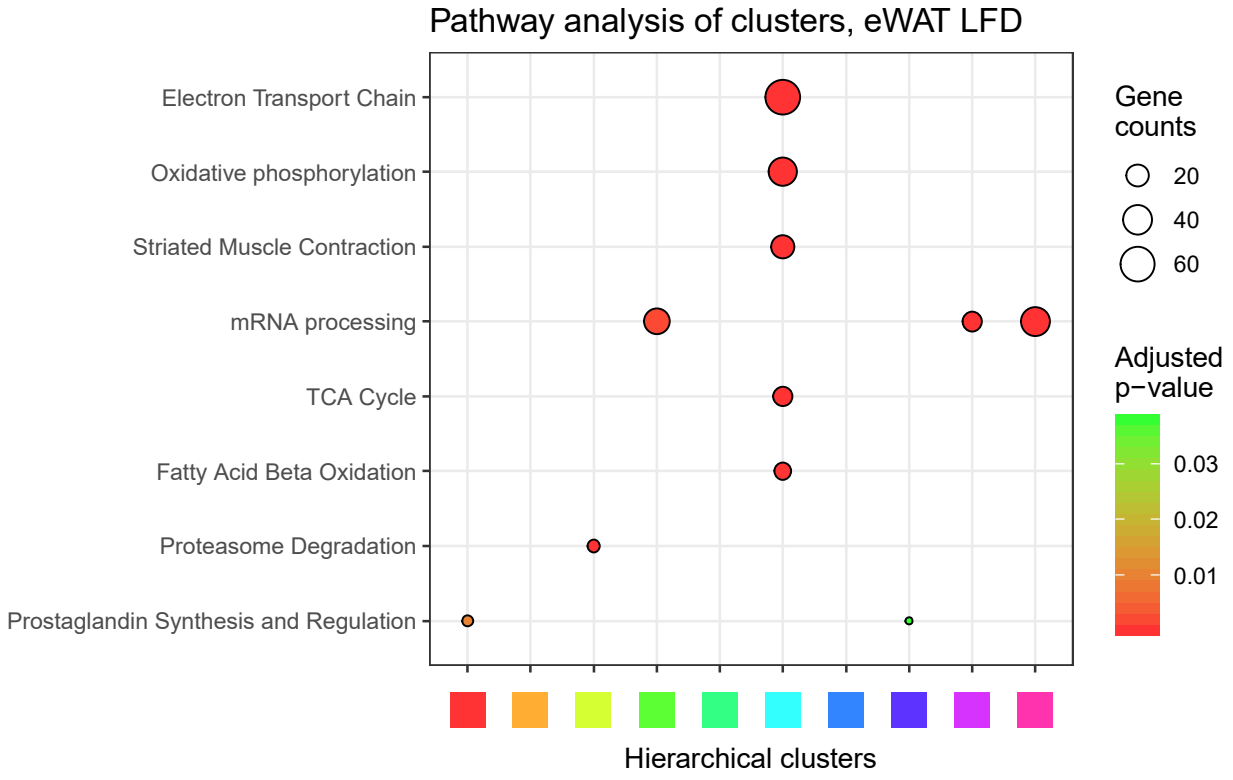

Figure 9. Pathway analysis of gene clusters defined through hierarchical clustering of significant differentially expressed genes in the low fat diet intervention group. Horizontally are the gene clusters as seen in Figure 10. Vertically are the names of the top 5 pathways associated with the significant differentially expressed genes in each cluster. Each point represents a pathway in a cluster, sized according to the number of genes associated with the pathway and coloured according to the adjusted probability value. The adjusted probability values are determined using the Benjamini–Hochberg procedure of false discovery rate.

hierarchical clusters is performed relative to the WikiPathways reference database (137). An alternative to the WikiPathways reference database is the Kyoto Encyclopedia of Genes and Genomes (KEGG) pathway reference database (138). The KEGG pathway reference database is, however, infrequently updated according to known literature relative to the WikiPathways reference database.

The top five pathways associated with genes of each cluster are illustrated in a dot plot (Figure 9). Each point represents a pathway in a cluster, sized according to the number of differentially expressed genes associated with the pathway and coloured according to the adjusted probability value. The adjusted probability values are determined using the Benjamini–Hochberg procedure of false discovery rate (139).

The cluster with the most significant differentially expressed genes is cluster six, whose genes are associated with pathways associated with the electron transport chain, oxidative phosphorylation, striated muscle contraction, tricarboxylic acid cycle also known as the citric acid cycle, and fatty acid beta oxidation (Figure 9). The genes in cluster four, nine and ten are associated with mRNA processing, whereas the genes of cluster three are associated with proteasome degradation (Figure 9). The genes in cluster one and eight are associated with processes of prostaglandin synthesis and regulation (Figure 9). Interestingly, many of the significant differentially expressed genes are associated with metabolic and mRNA processing pathways, suggesting that eWAT of mice with an age of ten weeks is still undergoing many developmental transcriptional changes. As only few significant differentially expressed genes were identified for iWAT, either caused by the high variance between iWAT sample replicates or by the suggestion that iWAT of mice with an age of ten weeks is fully developed, ageing-associated transcriptional changes are not identifiable. Further analyses are required to uncover the main cause of the lack of ageing-associated transcriptional changes of iWAT.

In summary, 3030 unique differentially expressed genes are identified between the eWAT LFD and week zero samples. Of these 3030 unique differentially expressed genes, 878 are significantly upregulated and 2152 are significantly downregulated. Between the iWAT LFD and week zero samples, 160 unique significant differentially expressed genes are identified, of which 88 of these are significantly upregulated and 72 are significantly downregulated. A pathway analysis of the differentially expressed genes for the eWAT conditions, revealed that they encode genes associated with metabolism, mRNA processing, proteasome degradation along with prostaglandin synthesis and regulation.

HFD exposure induces transcriptional changes of both eWAT and iWAT in mice

To investigate the impact of HFD exposure on adipocyte genes of eWAT and iWAT, and to verify their identity as adipose tissues, selected adipose tissue and adipocyte marker genes were plotted (Figure 11). The groupings of the bar plots are visualized according to time of sacrifice and diet group.

The genes that were selected in order to tissue identity are *Adipoq*, *Erg*, *Ets2*, *Fabp4*, *Lep*, *Lpl*, *Plin1*, *Pnpla2* and *Pparg* that encodes ADIPOQ, ERG, ETS2, FABP4, LEP, LPL, PLIN1, ATGL and PPARγ, respectively. *Adipoq* and *Lep* are chosen as they are important adipokines; *Erg, Ets2* and *Pparg* are chosen as they are transcription factors (TFs) involved in adipogenesis, amongst others; *Fabp4, Lpl, Plin1* and *Pnpla2* are chosen considering they involved in lipid metabolism.

Only the expression level of *Lep* changes significantly from eWAT week zero to eWAT week six HFD (Figure 11A). The expression levels of *Adipoq, Erg, Fabp4, Plin1, Pnpla2* and *Pparg* from the eWAT week twelve HFD samples are significantly lower relative to the LFD group (Figure 11A), while considered being unchanged or marginally decreased between the eWAT week six HFD and LFD samples (Figure 11A). The transcriptional changes in eWAT suggest increased lipid mobilisation (47) and tissue inflammation (47) along with decreased lipolytic activity (47, 48, 54) of the adipocytes in the eWAT. The significantly decreased expression levels of *Fabp4* and *Pparg* from the eWAT week twelve HFD samples relative to the week zero samples (Figure 11A), additionally suggest a decreased lipolytic activity (140) of the adipocytes of eWAT. No transcriptional changes between any of the eWAT samples are observed for *Ets2* and *Lpl* (Figure 11A). The transcriptional level of *Lep* is significantly increased from both the eWAT week six and twelve HFD samples relative to the week zero samples (Figure 11A), while the transcriptional changes of *Lep* between the eWAT HFD and LFD samples of both week six and twelve are not significant (Figure 11A). Increases in *Lep* transcription indicates increased storage of lipids.

Opposite of the eWAT samples, most of the selected genes show transcriptional increases between the HFD samples relative to the LFD samples in the iWAT (Figure 11B). The transcriptional levels of *Erg, Ets2, Fabp4, Lep* and *Lpl* are significantly increased in iWAT week twelve HFD samples relative to LFD samples (Figure 11B). Additionally, the transcriptional levels of *Ets2, Lip* and *Lpl* are significantly increased in iWAT week twelve HFD samples relative to week zero samples (Figure 11B), all of which suggest increased adipocytic lipid uptake from chylomicrons and VLDL (46) and AT expansion through hyperplasia (69). No transcriptional changes between iWAT samples are observed for *Adipoq, Plin1, Pnpla2* and *Pparg* (Figure 11B).

To summarise, the transcriptional changes of the selected genes in the eWAT suggest increased lipid mobilisation and tissue inflammation along with decreased lipolytic activity of the adipocytes, whereas the transcriptional changes of the selected genes in the iWAT suggest increased adipocytic lipid uptake and adipogenesis, suggesting that eWAT expands through hypertrophy and iWAT expands through hyperplasia.

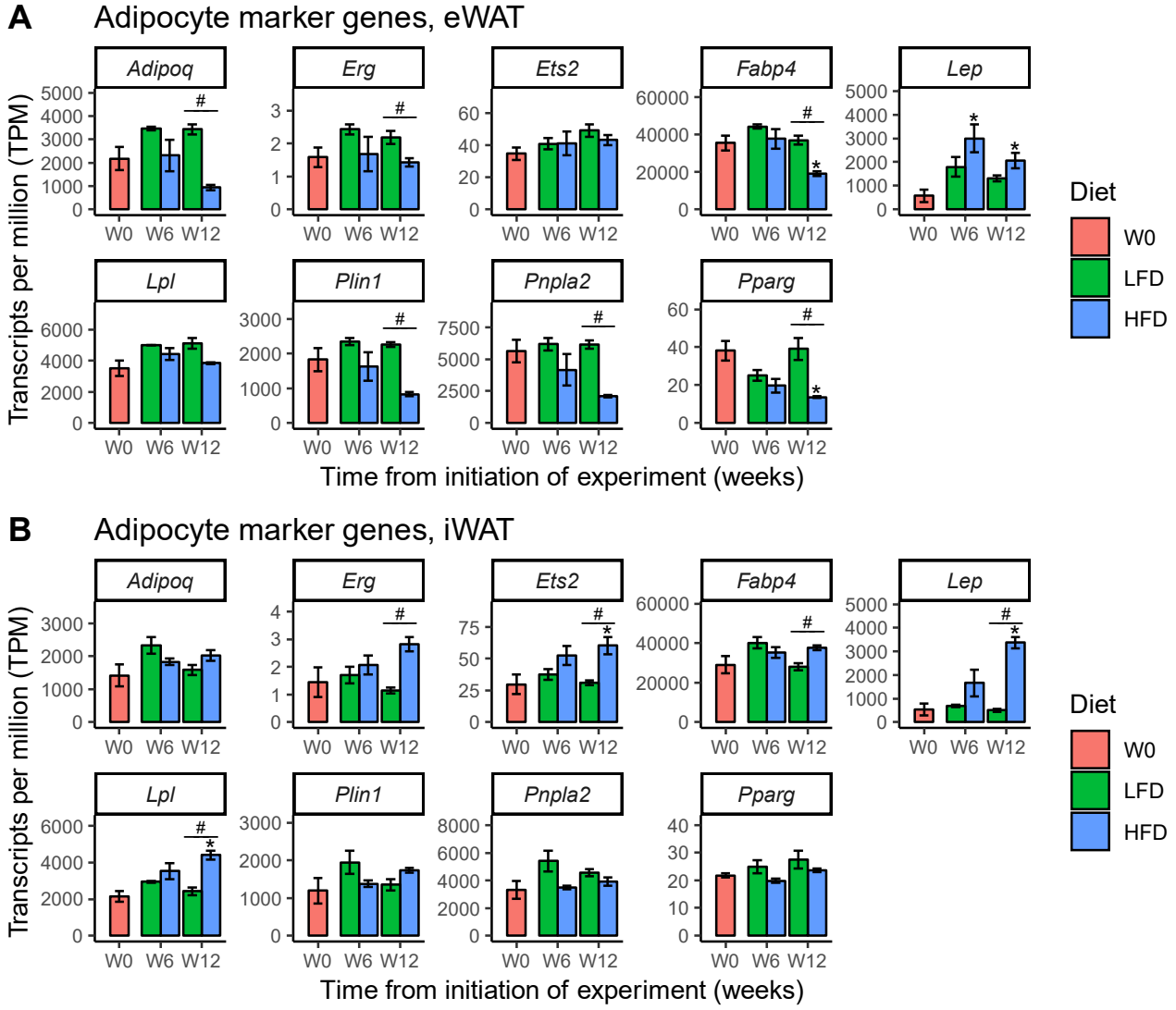

*Figure 11. Adipocyte identity marker genes. **(A)** Visualisations of adipocyte identity marker genes from eWAT presented as bar plots. Horizontally are the time points of which the mice were sacrificed. Vertically are the transcripts per kilobase million (TPM). **(B)** Visualisations of adipocyte identity marker genes from iWAT presented as bar plots. Horizontally are the time points of which the mice were sacrificed. Vertically are the transcripts per kilobase million (TPM). Gene transcript counts from week zero mice, are coloured in red, whereas gene transcript counts from mice fed with a LFD and a HFD are coloured in green and blue, respectively. Error bars indicate standard error of mean. All * denotations indicate that there is a significant difference between the mean at the indicated time point and week zero ($p < 0.05$). All # denotations indicate that there is a significant difference between the LFD and HFD means ($p < 0.05$), P values are calculated using a Student's t-test.*

Proportion of HFD-induced significant differential expressions increase with time

To investigate the DIO-related transcriptional changes in mouse adipose tissues, DE analyses are conducted tissue-wise on LFD and HFD samples from each time point after the initiation of the experiment (Figure 12). The following conditions were compared: eWAT week six HFD samples with eWAT week six LFD samples (Figure 12A); eWAT week twelve HFD samples with eWAT week twelve LFD samples (Figure 12B); iWAT week six HFD samples with iWAT week six LFD samples (Figure 12C); iWAT week twelve HFD samples with iWAT week twelve LFD samples (Figure 12D).

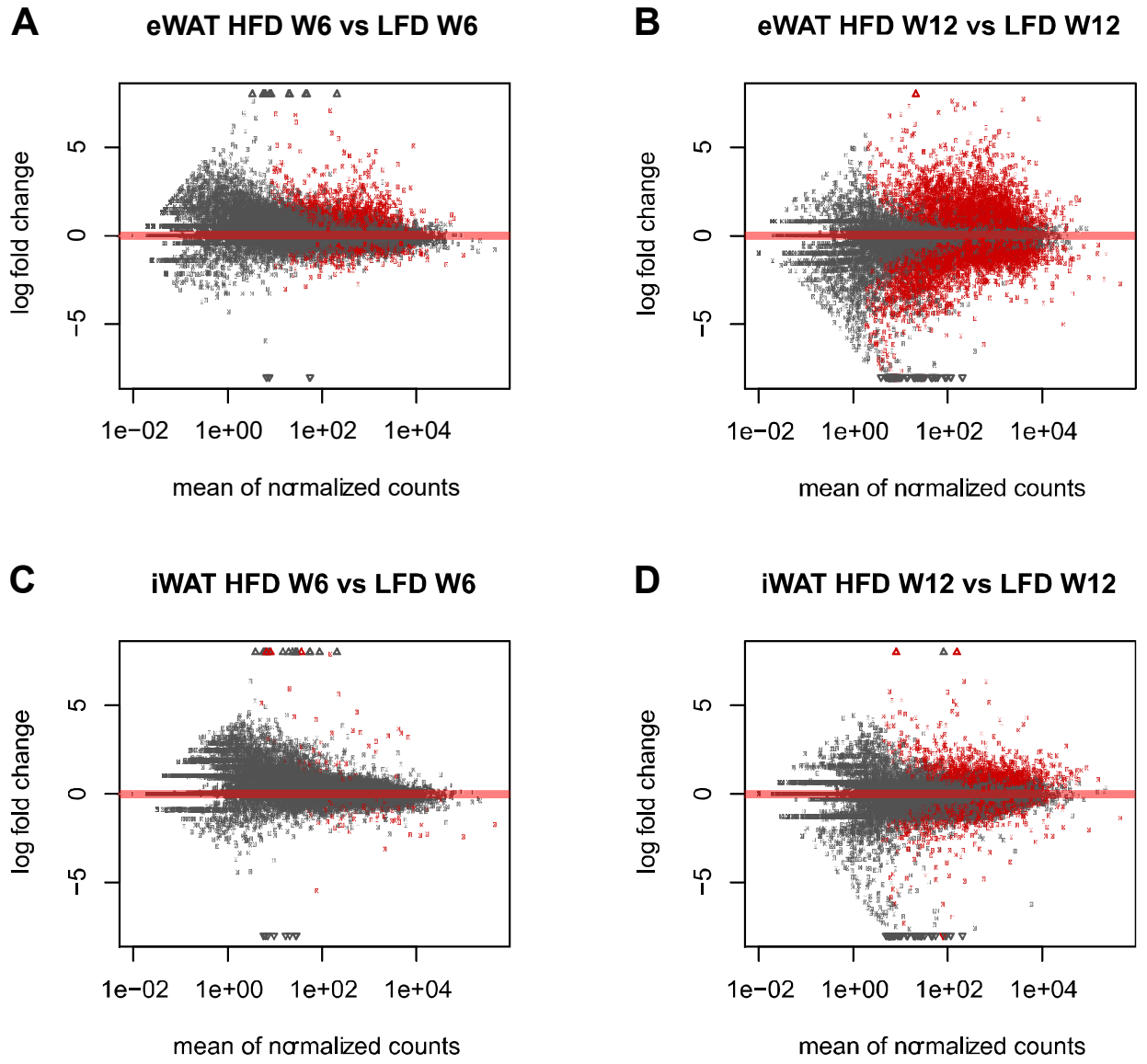

*Figure 12. Obesity induced transcriptional changes in mouse adipose tissue. Differential expression analyses of (**A**) eWAT week six HFD samples vs eWAT week six LFD samples, (**B**) eWAT week twelve HFD samples vs eWAT week twelve LFD samples, (**C**) iWAT week six HFD samples vs iWAT week six LFD samples, (**D**) iWAT week twelve HFD samples vs iWAT week twelve LFD samples. Vertically is the log2 fold change. Horisontally is the mean of the normalised counts. Significant (FDR < 0.05) and non-significant differentially expressed genes are coloured in red and grey, respectively. P-values are corrected for multiple testing by the Benjamini-Hochberg procedure.*

In total, 1003 significant transcriptional changes are observable between the eWAT week six HFD samples and the eWAT week six LFD samples, whereas 757 of these are significant upregulations and 246 are significant downregulations (Figure 12A). Increasingly, there are a total of 6496 significant transcriptional changes between the eWAT week twelve HFD samples and the eWAT week twelve LFD samples, whereas 3327 are significant upregulations and 3169 are significant downregulations (Figure 12B).

Between the iWAT week six HFD samples and the iWAT week six LFD samples there are a total of 71 significant transcriptional changes, whereof 24 are significant upregulations and 47 are significant downregulations (Figure 12C). Increasingly, there are 2195 significant transcriptional changes between the iWAT week twelve HFD samples and the iWAT week twelve LFD samples, of which 1263 are significant upregulations and 932 are significant downregulations (Figure 12D).

Seemingly, DIO-related significant expression differences are more abundant in eWAT than in iWAT, probably explained by large variances between iWAT sample replicates (Figure 6B). Additionally, the amount of significant expressional changes increases with the duration of HFD-exposure of the mice.

To further investigate the impact DIO has on the expression levels of genes in mouse adipose tissues, the significant differentially expressed genes are divided into clusters, tissue-wise (Figure 13).

The TPM values of the significant differentially expressed genes from the eWAT HFD and week zero samples increases over time in the red, lime green, spring green, and light blue clusters (Figure 13A), whereas they might encode pro-inflammatory and pro-fibrotic proteins. Opposite, the TPM values of the significant differentially expressed genes from the eWAT HFD and week zero samples decrease over time in the yellow, blue and purple clusters (Figure 13A), whereas they might encode anti-inflammatory and anti-fibrotic proteins. The TPM values of the significant differentially expressed genes from the eWAT samples in the orchid cluster increases from week zero to week six and decrease from week six to week twelve (Figure 13A).

The TPM values of the significant differentially expressed genes from the iWAT HFD and week zero samples increases over time in the red, lime green and spring green clusters (Figure 13B), suggestively encoding pro-adipogenic proteins. Whereas, the TPM values of the significant differentially expressed genes from the iWAT HFD and week zero samples decreases over time in the yellow, light blue and blue clusters (Figure 13B), suggestively encoding anti-adipogenic

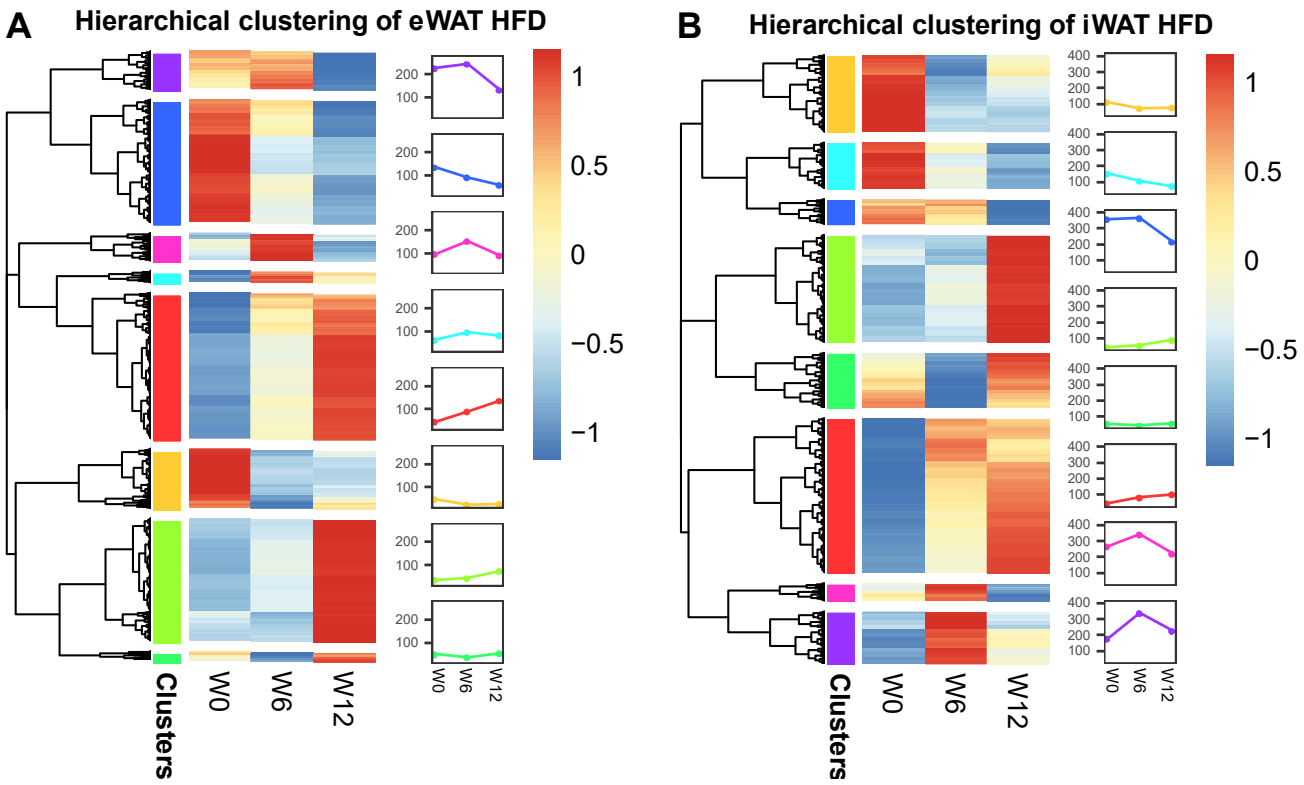

*Figure 13. Tissue-wise hierarchical clustering of significant differentially expressed genes. The significant differentially expressed genes from (**A**) eWAT and (**B**) iWAT are divided into eight clusters each. The clusters have been appointed appropriate colours according to the visible light spectrum (red, yellow, lime green, spring green, light blue, blue, purple and orchid). The genes are coloured according to TPM values that are scaled by row (for each gene). Adjacent to the hierarchical clusters are the mean TPM changes of the genes within each cluster plotted according to duration of HFD-exposure.*

proteins. The TPM values of the significant differentially expressed genes from the iWAT samples in the purple and orchid clusters increases from week zero to week six and decrease from week six to week twelve (Figure 13B). Additionally, the decrease in the TPM values from week six to week twelve observed for the genes in the purple and orchid clusters resemble the decrease in TPM values from week six to week twelve observed for the genes in the blue cluster (Figure 13B).

Pathway analyses are conducted on the genes in each cluster, tissue-wise. The pathway analyses of the hierarchical clusters are performed relative to the WikiPathways reference database. The top five pathways associated with genes of each cluster are visualised in dot plots for eWAT HFD samples (Figure 14) and iWAT HFD samples (Figure 15). Each point represents a pathway in a cluster, sized according to the number of genes associated with the pathway and coloured according to the adjusted probability value. The adjusted probability values are determined using the Benjamini–Hochberg procedure of false discovery rate.

The significant differentially expressed genes in the red cluster, determined from the eWAT samples, are associated with the following pathways: IL-3 signalling, spinal cord injury, microglia pathogen phagocytosis, DNA replication and TYROBP casual network (Figure 14); all of which are related to inflammatory responses and proliferation of immune cells (137, 141). The pathways of the red cluster non the less have adjusted probability values of less than 0.01, whereas it is unlikely that they have occurred by chance (Figure 14). The significant differentially expressed genes in the lime green cluster are associated with pathways including chemokine signalling, EGFR1 signalling, insulin signalling, kit receptor signalling and TYROBP casual network, and have adjusted probability values of less than 0.01 (Figure 14). The mentioned pathways from the lime green cluster are associated with inflammatory responses,

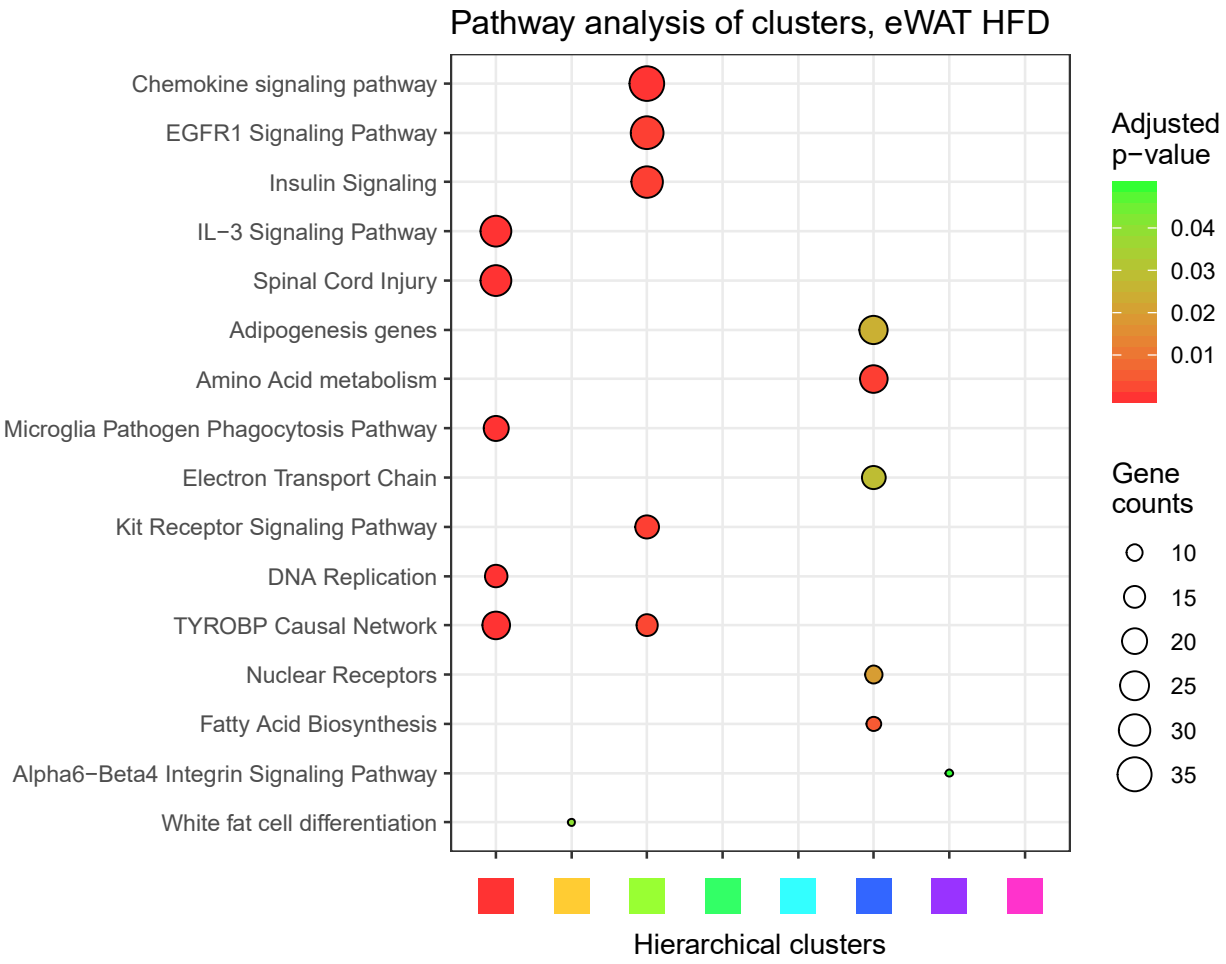

Figure 14. Pathway analysis of gene clusters defined through hierarchical clustering of significant differentially expressed genes in the eWAT high fat diet group. Horizontally are the gene clusters as in Figure 13A. Vertically are the names of the top 5 pathways associated with the significant differentially expressed genes in each cluster. Each point represents a pathway in a cluster, sized according to the number of genes associated with the pathway and coloured according to the adjusted probability value. The adjusted probability values are determined using the Benjamini–Hochberg procedure of false discovery rate.

the formation of immune cells such as lymphocytes, and insulin signalling in general (137). Both the genes in the red and lime green cluster are upregulated during DIO (Figure 13A). The genes in the blue cluster are downregulated in response to DIO (Figure 13A). Pathways associated with genes in the blue cluster include adipogenesis genes, amino acid metabolism, electron transport chain, nuclear receptors, and fatty acid biosynthesis, and have adjusted probability values of less than 0.03 (Figure 14). These pathways are involved in the adipogenesis and metabolic processes (137, 141). Significant differentially expressed genes in the purple and yellow clusters are involved in the following pathways: alpha6-beta4 integrin signalling and white fat cell differentiation, respectively (Figure 14). The alpha6-beta4 integrin signalling pathway has an adjusted probability value greater than 0.04 (Figure 14) and is involved in mediating signals from the ECM (125, 137). The pathways of white fat cell differentiation have a probability value between 0.04 and 0.03 (Figure 14) and are involved in adipogenesis (137). The genes in the spring green, light blue and orchid clusters are not associated with any currently known pathways (Figure 14). Overall, the pathways associated with significant differentially expressed genes, determined through DE analyses of combinations of the eWAT HFD and week zero samples, suggest that DIO causes upregulation of pro-inflammatory genes and perhaps some pro-fibrotic genes along with downregulation of genes involved in adipogenic and metabolic processes in the eWAT.

The significant differentially expressed genes in the red cluster, determined through DE analyses of the iWAT HFD and week zero samples, are associated with pathways including focal adhesion-PI3K-Akt-mTOR-signalling, primary focal segmental glomerulosclerosis along with prostaglandin synthesis and regulation (Figure 15); they all have adjusted probability values of approximately 0.03 (Figure 15). The beforementioned pathways are involved in cell proliferation, differentiation and paracrine signalling, along with tissue growth (137). The genes of the yellow cluster are associated with mRNA processing (Figure 15); the process has an adjusted probability value of approximately 0.02 (Figure 15). The significant differentially expressed genes in the spring green cluster are additionally associated with mRNA processing, with an adjusted probability value of less than 0.01, along with cytoplasmic ribosomal proteins, with an adjusted probability value of approximately 0.01 (Figure 15). The genes in the light blue and blue clusters are additionally associated with cytoplasmic ribosomal proteins, with adjusted probability values approximately equal to or less than 0.01, respectively (Figure 15). The genes in the light green cluster are also associated with pathways of cytoplasmic ribosomal proteins in

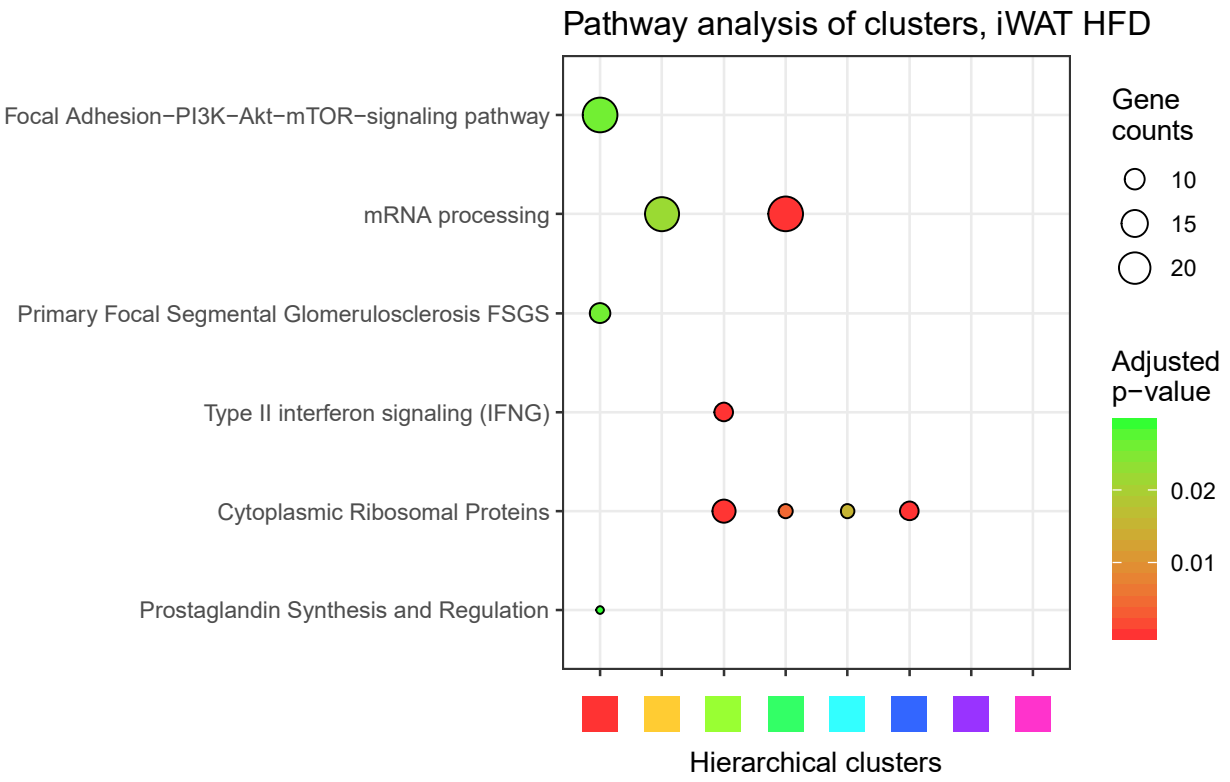

Figure 15. Pathway analysis of gene clusters defined through hierarchical clustering of significant differentially expressed genes in the iWAT high fat diet group. Horizontally are the gene clusters as in figure 13B. Vertically are names of the top 5 pathways associated with the significant differentially expressed genes in each cluster. Each point represents a pathway in a cluster, sized according to the number of genes associated with the pathway and coloured according to the adjusted probability value. The adjusted probability values are determined using the Benjamini–Hochberg procedure of false discovery rate.

addition to type II interferon signalling (IFNG) (Figure 15), proposedly suggesting a marginally inflammatory state of the iWAT (137); both of these pathways have adjusted probability values of less than 0.01 (Figure 15).

To summarise; the pathways associated with the significant differentially expressed genes, determined through DE analyses of eWAT HFD and week zero samples, suggest that DIO causes inflammation, increased immune cells proliferation along with decreases in metabolic pathways and probably inhibition of adipogenesis in the eWAT; the pathways associated with the significant differentially expressed genes, determined through DE analyses of iWAT HFD and week zero samples, suggest that DIO causes increased adipogenic AT expansion and probably a slightly inflammatory state in the iWAT; additionally, prolonged HFD-exposure probably leads to exacerbation of DIO-related complications.

Increased expression of inflammation marker genes in eWAT but not iWAT

To investigate the inflammatory state of the tissues, selected inflammation marker genes were plotted in bar plots (Figure 16A-B). The groupings of the bar plots are visualised according to time of sacrifice and diet group as in previous bar plots.

The transcriptional levels of *adhesion G protein-coupled receptor E1 (Adgre1)* and *integrin alpha M* (*Itgam)* are used as indicators of macrophage presence, whereas the transcriptional levels of *Cd4* and *Cd8a* are used as indicators of the presence of T helper cells (Th) and cytotoxic T cells, respectively. The transcriptional levels of *Ccl2, C-X-C motif chemokine 12 (Cxcl12), Il1b, Nfkb1* and *Tnf* are used as indicators of general inflammation. *Interferon gamma (Infg)* and *Il2* are used as an indicator of Th1 presence, *Il2, Il4, Il5* and *Il10* are used as indicators of Th2 presence, while *Il6* is used as an indicator of Th17 presence.

The transcriptional levels of the macrophage marker genes in the eWAT are both increasing according to the amount of time the mice have been exposed to an HFD (Figure 16A). The increases in the transcriptional levels of the macrophage marker genes are significantly increased in the eWAT HFD samples relative to the eWAT LFD samples twelve weeks after the initiation of the experiment (Figure 16A), suggesting an obesity-related increased presence of macrophages in the eWAT. There is an increase in the transcriptional levels of the general inflammatory markers *Ccl2, Cxcl12, Il1b, Nfkb1* and *Tnf* in eWAT HFD samples relative to eWAT LFD samples; the transcriptional differences between the eWAT week twelve HFD and eWAT week twelve LFD samples of the general inflammatory markers are significant (Figure 16A), suggesting increased DIO-related inflammation. The T helper cell (*Cd4*) and cytotoxic T cell (*Cd8a*) markers are both considered not significant differentially expressed (Figure 16A). There is no transcriptional difference between the marker genes for Th1, Th2 and Th17 cells, except *Il10* (Figure 16A), this suggests little to no DIO-related proportional changes of the Th cells. The Th2 cell marker, *Il10*, is differentially expressed in eWAT week twelve HFD samples relative to eWAT week twelve LFD samples (Figure 16A). Interestingly, this suggests a power-struggle between pro-inflammatory and anti-inflammatory cells. The levels of the general inflammatory markers do, however, indicate that the pro-inflammatory cells are on the winning side, suggestively due to a cumulative effect of all released pro- and anti-inflammatory cytokines.

There are contradictory results regarding the transcriptional differences of the macrophage gene indicators; the transcriptional levels of *Adgre1* increase in iWAT HFD samples relative to iWAT LFD samples, while the transcriptional levels of *Itgam* do not change between the iWAT

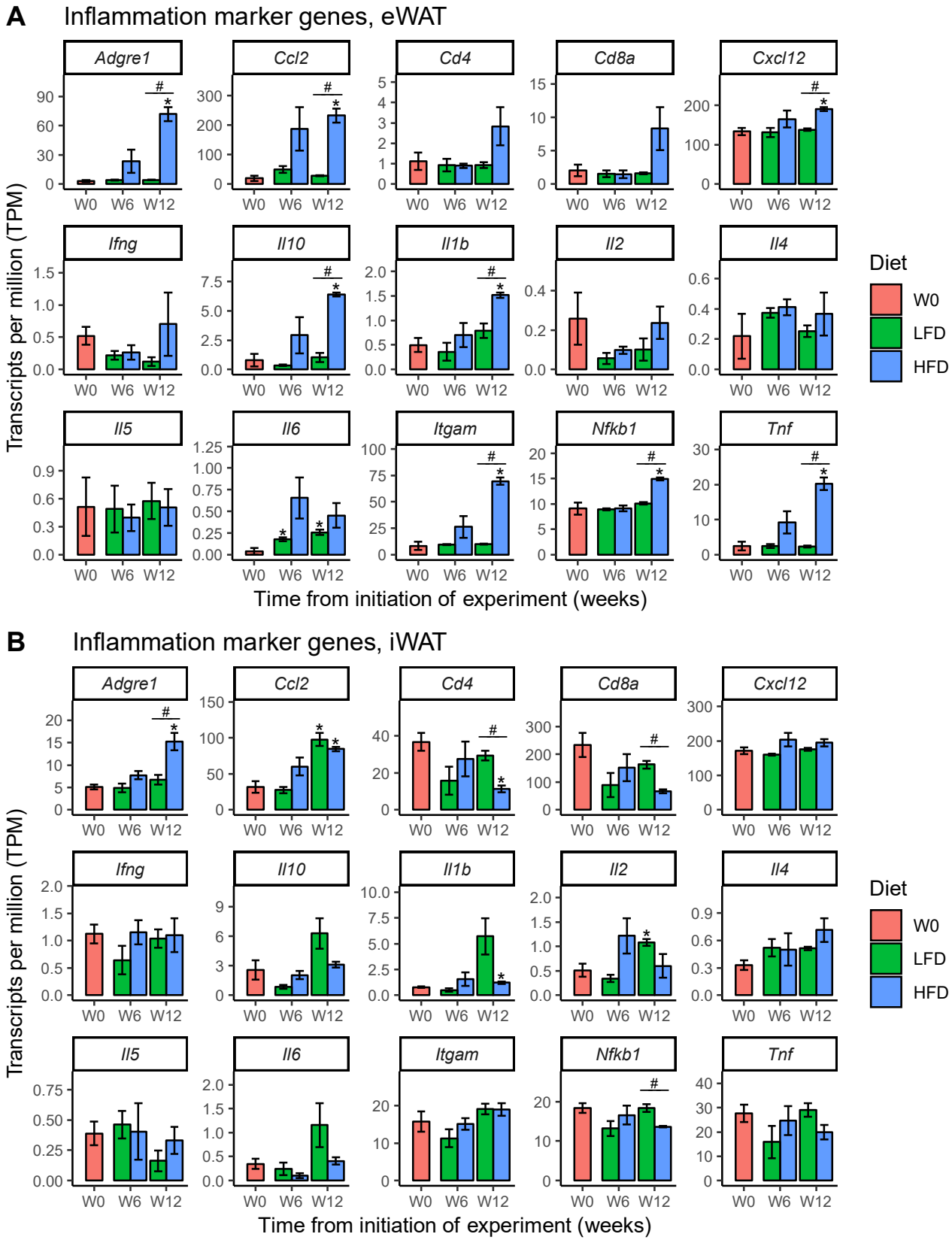
A
Inflammation marker genes, eWAT
Adgre1
Ccl2
Cd4
Cd8a
Cxcl12
Ifng
Il10
Il1b
Il2
Il4
Il5
Il6
Itgam
Nfkb1
Tnf
Transcripts per million (TPM)
W0 W6 W12
Time from initiation of experiment (weeks)
Diet
W0
LFD
HFD
B
Inflammation marker genes, iWAT
Adgre1
Ccl2
Cd4
Cd8a
Cxcl12
Ifng
Il10
Il1b
Il2
Il4
Il5
Il6
Itgam
Nfkb1
Tnf
Transcripts per million (TPM)
W0 W6 W12
Time from initiation of experiment (weeks)
Diet
W0
LFD
HFD

*Figure 16. Inflammation marker genes. (**A**) Visualisations of transcripts of inflammation marker genes from eWAT samples presented as bar plots. Horizontally are the times of which the mice were sacrificed. Vertically are the transcripts per kilobase million. (**B**) Visualisations of transcripts of inflammation marker genes from iWAT presented as bar plots. Horizontally are the times of which the mice were sacrificed. Vertically are the transcripts per kilobase million (TPM). Gene transcript counts from week zero mice, are coloured in red, whereas gene transcript counts from mice fed with a LFD and a HFD are coloured in green and blue, respectively. Error bars indicate standard error of mean. All * denotations indicate that there is a significant difference between the mean at the indicated time point and week zero ($p < 0.05$). All # denotations indicate that there is a significant difference between the LFD and HFD means ($p < 0.05$), P values are calculated using a Student's t-test.*

samples (Figure 16B). There are significant transcriptional differences of *Adgre1* between iWAT week twelve HFD samples and iWAT week twelve LFD samples in addition to between iWAT week twelve HFD samples and iWAT week zero samples (Figure 16B). There are significant transcriptional increases of the general inflammation marker, *Ccl2*, between the iWAT week twelve HFD samples and iWAT week zero samples in addition to between iWAT week twelve LFD samples and iWAT week zero samples (Figure 16B). There is an observable significant transcriptional difference of *Nfkb1* between the iWAT week twelve HFD and LFD samples (Figure 16B), which could suggest decreased iWAT inflammation. The transcriptional levels of *Cd4* and *Cd8a* from the iWAT week twelve HFD and LFD samples are significantly different from each other, in addition to the transcriptional levels of *Cd4* from the iWAT week twelve samples relative to the iWAT week zero samples (Figure 16B); this suggests a DIO-related proportional decrease of both T helper cells and cytotoxic T cells. There are seemingly no significant transcriptional differences between any of the T helper cell subtype-specific marker genes from the iWAT HFD and LFD samples from any given time point (Figure 16B). It is suggested that there might be a decrease in the amount of T helper and cytotoxic T cells presence in the iWAT, yet that the transcriptional levels of the Th subtype-defined cytokines are maintained by immune cells other than Th cells, possibly cytokine producing Th-like B2 cells.

In summary, the eWAT seems to be highly inflamed, whereas the iWAT does not. The absence of inflammation in the iWAT is explainable by increased hyperplasic AT expansion. Additionally, there seem to be proportional changes to the immune cells in eWAT in response to DIO, while it is suggested that there are fewer proportional changes to the immune cells of iWAT.

Early development of fibrosis in eWAT but not iWAT

To investigate if the tissues are in a fibrotic state, selected fibrosis marker genes were plotted (Figure 17A-B). The groupings and the colouring of them are identical to those of the previous bar plots.

Col1a1, Col3a1 and *Col6a1* are commonly considered pro-fibrotic collagens (125), whereas they will be used as indicators of a switch in ECM composition in addition to *Mmp2, Mmp9* and *Mmp14*. *Decorin (Dcn)* and *fibronectin (Fn1)* are ECM adhesion proteins (125) and will be used as an indicator of ECM-cell adhesions. *Dcn* will further be used as an indicator of ECM abundance, as it is involved in the folding of ECM components (125). *Hif1a* will be used as an indicator of early ECM remodelling, whereas *Ctgf, Lysyl oxidase (Lox)* and *Tgfb1* will be used as general indicators of fibrosis. *Lox* will in addition to *Dcn* be used as an indicator of ECM abundance, due to its ability to cross-link collagens (125). It is observed that all fibrosis marker genes, expect for *Ctgf* and *Mmp9*, are significantly upregulated in eWAT week twelve HFD samples relative to eWAT week twelve LFD samples; all of these, except for *Dcn*, are also significantly upregulated in eWAT week twelve HFD samples relative to eWAT week zero samples (Figure 17A). *Col6a1* is additionally significantly upregulated in eWAT week six HFD samples relative to eWAT week zero samples (Figure 17A). All of which suggests that there has been a shift in the ECM composition to a more stiff ECM and that there is an increased abundance of the ECM components. Additionally, it is suggested that the turnover of ECM components is modulated, due to the transcriptional increase of *Mmp2* and *Mmp14* and the transcriptional decrease of *Mmp9* (Figure 17A). The transcriptional levels of *Ctgf* are significantly decreased in eWAT week six HFD samples relative to eWAT week six LFD samples, but not between eWAT week twelve HFD and LFD samples (Figure 17A). *Ctgf* is considered to be important if not essential for the development of fibrosis in multiple organs (125), whereas it can be postulated to likewise have an important role in the development of AT fibrosis. The significant downregulation of *Ctgf* in eWAT week six HFD samples relative to eWAT week six LFD samples is interesting, especially as the transcriptional level evens out in the eWAT week twelve samples (Figure 17A). It is proposed that the onset of fibrosis in the eWAT occurs within the experimental timeframe; however, that prolonged HFD exposure is required to develop fibrosis in the eWAT.

Genes including *Col1a1, Col3a1, Col6a1* and *Hif1a* are significantly upregulated in iWAT week twelve HFD samples relative to iWAT week twelve LFD samples (Figure 17B), suggesting an early ECM remodelling in response to a hypoxic environment; *Hif1a* is also significantly upregulated in iWAT week six HFD samples relative to iWAT week six LFD samples (Figure 17B). The transcriptional levels of the beforementioned genes are also significantly upregulated in iWAT week twelve HFD samples relative to iWAT week zero samples (Figure 17B). *Col6a1* is also significantly upregulated in iWAT week six samples relative to iWAT week zero samples, while

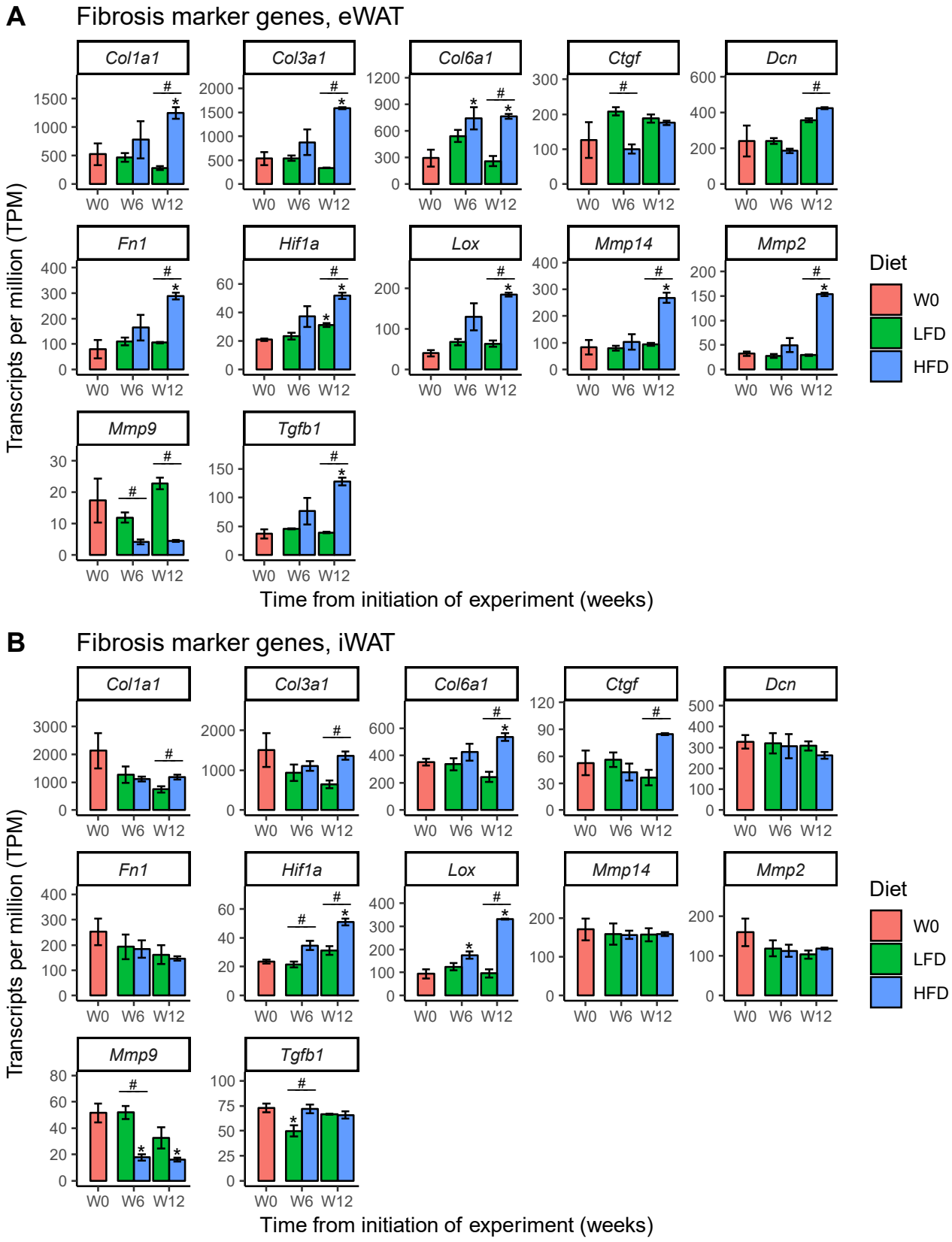
A
Fibrosis marker genes, eWAT
Col1a1
Col3a1
Col6a1
Ctgf
Dcn
Fn1
Hif1a
Lox
Mmp14
Mmp2
Mmp9
Tgfb1
W0 W6 W12
Transcripts per million (TPM)
Time from initiation of experiment (weeks)
Diet
W0
LFD
HFD
B
Fibrosis marker genes, iWAT
Col1a1
Col3a1
Col6a1
Ctgf
Dcn
Fn1
Hif1a
Lox
Mmp14
Mmp2
Mmp9
Tgfb1
W0 W6 W12
Transcripts per million (TPM)
Time from initiation of experiment (weeks)
Diet
W0
LFD
HFD

*Figure 17. Fibrosis marker genes. (**A**) Visualisations of transcripts of fibrosis marker genes from eWAT samples presented as bar plots. Horizontally are the times of which the mice were sacrificed. Vertically are the transcripts per kilobase million. (**B**) Visualisations of transcripts of fibrosis marker genes from iWAT presented as bar plots. Horizontally are the times of which the mice were sacrificed. Vertically are the transcripts per kilobase million. Gene transcript counts from week zero mice, are coloured in red, whereas gene transcript counts from mice fed with a LFD and a HFD are coloured in green and blue, respectively. Error bars indicate standard error of mean. All * denotations indicate that there is a significant difference between the mean at the indicated time point and week zero ($p < 0.05$). All # denotations indicate that there is a significant difference between the LFD and HFD means ($p < 0.05$), P values are calculated using a Student's t-test.*

Hif1a is significantly upregulated in iWAT week twelve samples relative to iWAT week zero samples (Figure 17B). Upregulation of *Hif1a* in iWAT could indicate that iWAT not only expands through hyperplasia, but also hypertrophy. *Ctgf* is significantly upregulated in iWAT week twelve HFD samples relative to iWAT week twelve LFD samples, and *Tgfb1* is significantly upregulated in iWAT week six HFD samples relative to iWAT week six LFD samples (Figure 17B); both of which suggest that there is ongoing tissue remodelling, possibly even onsetting fibrosis. The transcriptional levels of *Lox* are significantly upregulated in iWAT week twelve HFD samples relative to iWAT week twelve LFD samples, along with in iWAT week six and twelve HFD samples relative to iWAT week zero samples (Figure 17B), suggesting DIO-related increase in collagen cross-linking. The transcriptional levels of the genes *Dcn, Fn1, Mmp2* and *Mmp14* do not significantly change among any of the iWAT samples (Figure 17B). Increased abundance of some of the beforementioned genes is known to be associated with the development of fibrosis, whereas their transcriptional levels indicate that fibrosis is not under development in the iWAT. The transcriptional levels of *Mmp9* are significantly decreased in iWAT week six HFD samples relative to iWAT week six LFD samples, along in iWAT week six and twelve HFD samples relative to iWAT week zero samples. No significant transcriptional difference is observable for *Mmp9* between iWAT week twelve HFD and LFD samples. The expressions of *Mmp9* indicate that DIO might have an early effect on the transcriptional levels of *Mmp9*.

To summarise, DIO seemingly causes hypoxia in both eWAT and iWAT in addition to hypoxia-related remodelling of the ECM. The ECM of the eWAT seems to be subjected to more extensive remodelling than the iWAT. The lack of significant differential expression of genes encoding adhesion proteins and MMPs between the iWAT samples, but not the eWAT samples, suggest that the turnover of ECM components attribute to the development of fibrosis. Additionally, only eWAT seems to be in the early process of developing fibrosis in response to twelve weeks of HFD exposure.

Identification of fibrosis-related transcription factors

To identify potential TFs that might be important in the development of DIO-related fibrosis, a list of known human TFs from Integrated analysis of Motif Activity and Gene Expression changes of transcription factors (IMAGE) (142) is converted to mouse TFs and cross-referenced with the significant differentially expressed genes of the time-course experiment. Here, only eWAT is considered, as only few significant regulated genes were identified for iWAT. Cross-referring the list of TFs from IMAGE with genes that are significantly regulated across time points yielded a list of 339 significant TFs that might be important drivers of for example early fibrosis development in eWAT.

To narrow the list down even further, the motif activity of the identified TFs were analysed using the computational tool Integrated System for Motif Activity Response Analyses (ISMARA) (134). ISMARA returned 207 TFs along with motif activities, which was subjected to hierarchical clustering factors (Figure 18) in order to identify patterns of TF motif activities. The motif activity of the TFs in the red cluster is increasing over time (Figure 18); the motif activity of the TFs in the yellow cluster increases from week zero to week six and decreases from week six to week twelve (Figure 18); the motif activity of the TFs in the green cluster decreases over time (Figure 18); the motif activity of the TFs in the blue cluster increases from week zero to week

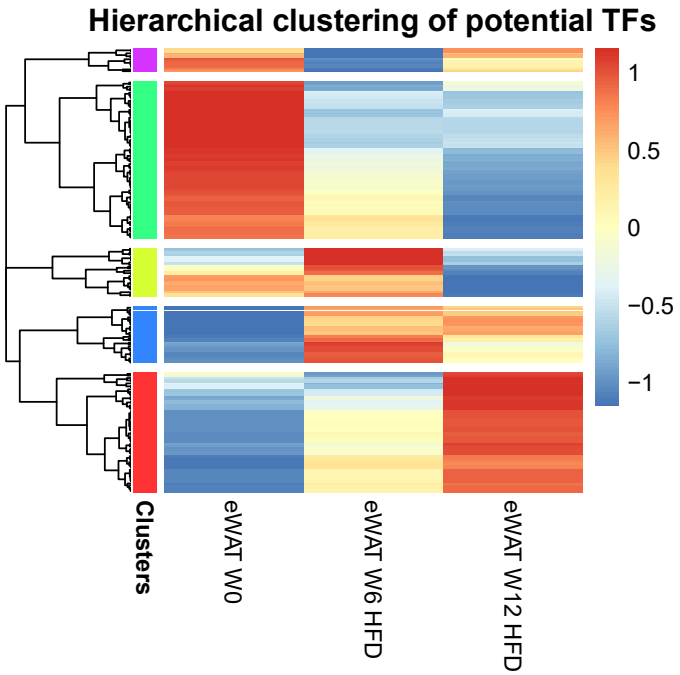

Figure 18. Hierarchical clustering of significant differentially expressed transcription factors encoding transcription factors that potentially are important for diet-induced obesity-related fibrosis in eWAT. The significant differentially expressed genes are divided into five clusters. The clusters have been appointed appropriate colours according to the visible light spectrum (red, yellow, green, blue and purple). The genes on the heatmap are coloured according to motif activity values from an ISMARA analysis that are scaled by row (for each gene).

six, and decreases from week six to the week twelve (Figure 18); the motif activity of the TFs in cluster five decreases from week zero to week six, and increases from week six to week twelve (Figure 18).

To identify which clusters contain genes potentially involved in the early development of fibrosis, a pathway analysis is performed on the genes in each cluster relative to the WikiPathways reference database. The pathways associated with genes of each cluster are illustrated in a dot plot (Figure 19).

The TFs of the red cluster are associated with the following processes from the WikiPathways reference database: focal adhesion-PI3K-Akt-mTOR-signalling, primary focal segmental glomerulosclerosis along with prostaglandin synthesis and regulation (Figure 19). The remaining clusters contain TFs involved in mRNA processing, type II interferon signalling in addition to cytoplasmic ribosomal proteins (Figure 19). The red cluster contains 61 TFs and is the strongest candidate for containing TFs involved in the early development of fibrosis. These TFs are listed in a table (Table 1) and ranked according to the importance of the motifs of the

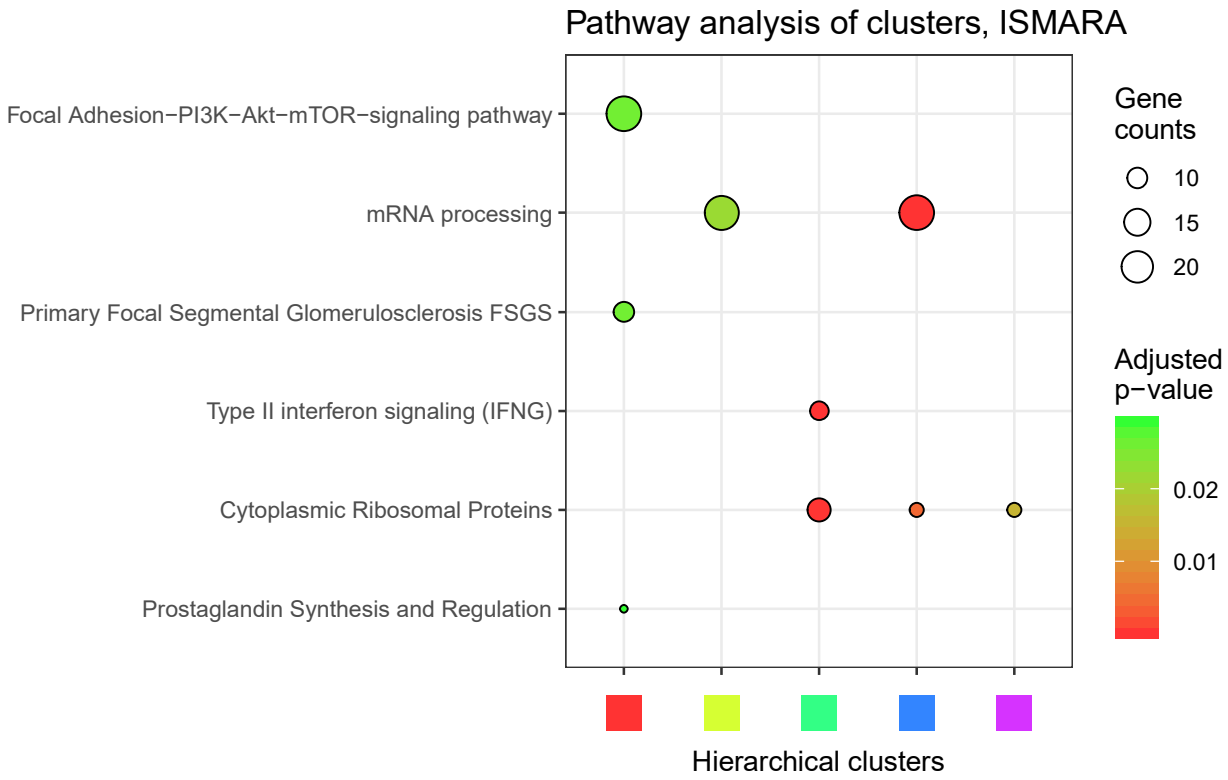

Figure 19. Pathway analysis of gene clusters defined through hierarchical clustering of significant differentially expressed transcription factors in the high fat diet group. Horizontally are the gene clusters as seen in Figure 18. Vertically are the names of the pathways associated with the significant differentially expressed genes in each cluster. Each point represents a pathway in a cluster, sized according to the number of genes associated with the pathway and coloured according to the adjusted probability value. The adjusted probability values are determined using the Benjamini–Hochberg procedure of false discovery rate.

	Gene symbol	Significance		Gene symbol	Significance		Gene symbol	Significance
1	Spi1	7.708204	23	E2f3	2.061875	45	Klf15	0.632309
2	Spic	6.726792	24	Hoxd9	1.956608	46	Nfkb2	0.608011
3	E2f2	4.768437	25	Fos	1.933533	47	Hoxd10	0.593620
4	Tfeb	4.195818	26	Sox10	1.706079	48	Mecom	0.562360
5	Srebf1	4.195818	27	Tcf4	1.631428	49	Thra	0.561779
6	Usf2	4.195818	28	Gsc	1.574483	50	Hoxc10	0.559648
7	Usf1	4.195818	29	E2f8	1.483798	51	Gata6	0.550883
8	Nfkb1	3.074219	30	Foxp2	1.469449	52	Alx4	0.549593
9	Rel	3.074219	31	Tcf7l2	1.446891	53	Zfp652	0.463805
10	Runx2	2.853135	32	Zbtb4	1.437698	54	Id4	0.459128
11	Elf1	2.811837	33	Nfix	1.262048	55	Pou3f3	0.385962
12	Elf2	2.811837	34	Zfp143	1.246625	56	Gzf1	0.384026
13	Elf4	2.811837	35	Smarcc2	1.246625	57	Hoxc4	0.282234
14	Irf8	2.626542	36	Six5	1.246625	58	Msx2	0.277152
15	Xbp1	2.326791	37	Sox4	1.143136	59	Foxd3	0.265851
16	Runx1	2.320822	38	Stat6	1.127362	60	Plagl1	0.182722
17	E2f1	2.308149	39	Homez	1.006333	61	Cdc5l	0.099108
18	Hmga1	2.245060	40	Egr1	0.973112			
19	Mybl2	2.198223	41	Fosb	0.936059			
20	Rora	2.174508	42	Prrx1	0.911639			
21	Egr2	2.087807	43	Batf	0.749740			
22	Tfdp1	2.087807	44	Trp63	0.713989			

Table 1. List of potential transcription factors that could be important in regulating diet-induced obesity-related fibrosis in eWAT. The transcription factors are determined through cross-referencing of significant differentially expressed genes encoding transcription factors with the ISMARA data output, followed by hierarchical clustering of the transcription factors with their motif activities (ISMARA output). Left of the transcription factor symbols are the ranking number. Right of the transcription factor symbols are the Z-score of the transcription factors, which summarises the importance of the motifs of the transcription factors for explaining the expression variance of the samples.

transcription factors for explaining the expression variance of the samples. The yielded list of TFs that might have an important role in driving the early stages DIO-associated fibrosis development, could be evaluated according to known literature and subjected to experiments, to assess their roles in driving the early stages DIO-associated fibrosis development.

Conclusion

Through analyses of transcriptional data of the epididymal white adipose tissue (eWAT) and the inguinal white adipose tissue (iWAT) over time from low fat diet (LFD) fed and high fat diet (HFD) fed male CL57BL/6J mice, it is suggested that eWAT expands through hypertrophy and that iWAT dominantly expands through hyperplasia in response to diet-induced obesity (DIO). Through pathway analyses of differentially expressed genes in addition to visualisation of specific inflammation and fibrosis marker genes, it is suggested that eWAT of HFD fed mice is hypoxic, inflamed, and progressively developing fibrosis, whereas iWAT of HFD fed mice is

hypoxic and marginally inflamed, only. It is suggested that what drives the development of fibrosis is not only increased extracellular matrix (ECM) component deposition but also modulated turnover of ECM components, through differential expression of matrix metalloproteinases (MMPs) such as MMP2, MMP9 and MMP14, adhesion proteins including decorin and fibronectin, collagens including collagen type I, III and VI, amongst others. It is additionally thought that the transcription factor (TF) transforming growth factor beta has a central role in adipocytic fibrogenesis, as observed in other organs. Lastly, a list of 61 potentially fibrosis-related TFs were identified through cross-referencing of integrated motif activity response analysis (ISMARA) data with significant differentially expressed genes, hierarchical clustering of the motif activity of the TFs encoded by significant differentially expressed genes along with a pathway analysis of the genes of each cluster.

In future experiments, the timeframe of this projects experiment setup could be extended in order to characterise both the early and late stages of DIO-associated fibrosis. Complementary to the experiment, chromatin immunoprecipitation sequencing could be conducted to assess the genome-wide interactions of selected TFs to the DNA. Alternatively, a knock-out experiment could be set up to determine the role of a selected TF in the early and/or late stages of DIO-associated fibrosis.

The next step would be to evaluate the yielded list of TFs according to known literature and the importance of the motifs of the TFs for explaining the expression variance of the samples from this projects data, and to select a TF thought to be an important driver of development of DIO-associated fibrosis. Afterwards, ideas concerning a future experimental setup should be consulted with colleagues, in order to work out a realistic approach.

References

1. Chooi YC, Ding C, Magkos F. The epidemiology of obesity. Metabolism. 2019;92:6-10.
2. Abdelaal M, le Roux CW, Docherty NG. Morbidity and mortality associated with obesity. Ann Transl Med. 2017;5(7):161-.
3. Biener A, Cawley J, Meyerhoefer C. The High and Rising Costs of Obesity to the US Health Care System. Journal of general internal medicine. 2017;32(Suppl 1):6-8.
4. Singh GM, Danaei G, Farzadfar F, Stevens GA, Woodward M, Wormser D, et al. The Age-Specific Quantitative Effects of Metabolic Risk Factors on Cardiovascular Diseases and Diabetes: A Pooled Analysis. PLOS ONE. 2013;8(7):e65174.
5. Sasai H, Sairenchi T, Iso H, Irie F, Otaka E, Tanaka K, et al. Relationship between obesity and incident diabetes in middle-aged and older Japanese adults: the Ibaraki Prefectural Health Study. Mayo Clin Proc. 2010;85(1):36-40.

6. Czernichow S, Kengne AP, Stamatakis E, Hamer M, Batty GD. Body mass index, waist circumference and waist-hip ratio: which is the better discriminator of cardiovascular disease mortality risk?: evidence from an individual-participant meta-analysis of 82 864 participants from nine cohort studies. Obesity reviews : an official journal of the International Association for the Study of Obesity. 2011;12(9):680-7.
7. Lauby-Secretan B, Scoccianti C, Loomis D, Grosse Y, Bianchini F, Straif K. Body Fatness and Cancer — Viewpoint of the IARC Working Group. New England Journal of Medicine. 2016;375(8):794-8.
8. Anandacoomarasamy A, Caterson I, Sambrook P, Fransen M, March L. The impact of obesity on the musculoskeletal system. International Journal Of Obesity. 2007;32:211.
9. Anstey KJ, Cherbuin N, Budge M, Young J. Body mass index in midlife and late-life as a risk factor for dementia: a meta-analysis of prospective studies. Obesity Reviews. 2011;12(5):e426-e37.
10. Keller KB, Lemberg L. Obesity and the metabolic syndrome. American journal of critical care : an official publication, American Association of Critical-Care Nurses. 2003;12(2):167-70.
11. Han TS, Lean ME. A clinical perspective of obesity, metabolic syndrome and cardiovascular disease. JRSM cardiovascular disease. 2016;5:2048004016633371-.
12. Nielsen JJ. Characterization of fibrotic transcriptional signatures in mouse adipose tissue using RNA-Seq [Project description]: University of Southern Denmark; 2019.
13. Yadav A, Kataria MA, Saini V, Yadav A. Role of leptin and adiponectin in insulin resistance. Clinica chimica acta; international journal of clinical chemistry. 2013;417:80-4.
14. Riobo Servan P. Obesity and diabetes. Nutricion hospitalaria. 2013;28 Suppl 5:138-43.
15. Brassard P, Legault S, Garneau C, Bogaty P, Dumesnil JG, Poirier P. Normalization of diastolic dysfunction in type 2 diabetics after exercise training. Medicine and science in sports and exercise. 2007;39(11):1896-901.
16. Lakhani M, Fein S. Effects of obesity and subsequent weight reduction on left ventricular function. Cardiology in review. 2011;19(1):1-4.
17. Wanahita N, Messerli FH, Bangalore S, Gami AS, Somers VK, Steinberg JS. Atrial fibrillation and obesity--results of a meta-analysis. American heart journal. 2008;155(2):310-5.
18. Grundy SM, Brewer HB, Jr., Cleeman JI, Smith SC, Jr., Lenfant C. Definition of metabolic syndrome: report of the National Heart, Lung, and Blood Institute/American Heart Association conference on scientific issues related to definition. Arteriosclerosis, thrombosis, and vascular biology. 2004;24(2):e13-8.
19. Nomura DK, Long JZ, Niessen S, Hoover HS, Ng SW, Cravatt BF. Monoacylglycerol lipase regulates a fatty acid network that promotes cancer pathogenesis. Cell. 2010;140(1):49-61.
20. Rosen ED, Spiegelman BM. What we talk about when we talk about fat. Cell. 2014;156(1-2):20-44.
21. Ahmadian M, Duncan RE, Jaworski K, Sarkadi-Nagy E, Sul HS. Triacylglycerol metabolism in adipose tissue. Future lipidology. 2007;2(2):229-37.
22. Loft A, Forss I, Mandrup S. Genome-Wide Insights into the Development and Function of Thermogenic Adipocytes. Trends in endocrinology and metabolism: TEM. 2017;28(2):104-20.
23. Ye L, Wu J, Cohen P, Kazak L, Khandekar MJ, Jedrychowski MP, et al. Fat cells directly sense temperature to activate thermogenesis. Proceedings of the National Academy of Sciences of the United States of America. 2013;110(30):12480-5.

24. Ramage LE, Akyol M, Fletcher AM, Forsythe J, Nixon M, Carter RN, et al. Glucocorticoids Acutely Increase Brown Adipose Tissue Activity in Humans, Revealing Species-Specific Differences in UCP-1 Regulation. Cell Metab. 2016;24(1):130-41.
25. Roh HC, Tsai LTY, Shao M, Tenen D, Shen Y, Kumari M, et al. Warming Induces Significant Reprogramming of Beige, but Not Brown, Adipocyte Cellular Identity. Cell metabolism. 2018;27(5):1121-37.e5.
26. Collaboration NCDRF. Worldwide trends in body-mass index, underweight, overweight, and obesity from 1975 to 2016: a pooled analysis of 2416 population-based measurement studies in 128·9 million children, adolescents, and adults. Lancet (London, England). 2017;390(10113):2627-42.
27. Reggio S, Pellegrinelli V, Clément K, Tordjman J. Fibrosis as a Cause or a Consequence of White Adipose Tissue Inflammation in Obesity. Current Obesity Reports. 2013;2(1):1-9.
28. Choe SS, Huh JY, Hwang IJ, Kim JI, Kim JB. Adipose Tissue Remodeling: Its Role in Energy Metabolism and Metabolic Disorders. Front Endocrinol (Lausanne). 2016;7:30-.
29. Ghaben AL, Scherer PE. Adipogenesis and metabolic health. Nature reviews Molecular cell biology. 2019;20(4):242-58.
30. Siersbaek R, Nielsen R, Mandrup S. Transcriptional networks and chromatin remodeling controlling adipogenesis. Trends in endocrinology and metabolism: TEM. 2012;23(2):56-64.
31. Lefterova MI, Haakonsson AK, Lazar MA, Mandrup S. PPARγ and the global map of adipogenesis and beyond. Trends in Endocrinology & Metabolism. 2014;25(6):293-302.
32. Siersbaek R, Rabiee A, Nielsen R, Sidoli S, Traynor S, Loft A, et al. Transcription factor cooperativity in early adipogenic hotspots and super-enhancers. Cell reports. 2014;7(5):1443-55.
33. Siersbæk R, Nielsen R, John S, Sung M-H, Baek S, Loft A, et al. Extensive chromatin remodelling and establishment of transcription factor 'hotspots' during early adipogenesis. The EMBO Journal. 2011;30(8):1459-72.
34. Bi P, Yue F, Karki A, Castro B, Wirbisky SE, Wang C, et al. Notch activation drives adipocyte dedifferentiation and tumorigenic transformation in mice. The Journal of experimental medicine. 2016;213(10):2019-37.
35. Marangoni RG, Korman BD, Wei J, Wood TA, Graham LV, Whitfield ML, et al. Myofibroblasts in murine cutaneous fibrosis originate from adiponectin-positive intradermal progenitors. Arthritis & rheumatology (Hoboken, NJ). 2015;67(4):1062-73.
36. Plikus MV, Guerrero-Juarez CF, Ito M, Li YR, Dedhia PH, Zheng Y, et al. Regeneration of fat cells from myofibroblasts during wound healing. Science (New York, NY). 2017;355(6326):748-52.
37. Wang QA, Song A, Chen W, Schwalie PC, Zhang F, Vishvanath L, et al. Reversible De-differentiation of Mature White Adipocytes into Preadipocyte-like Precursors during Lactation. Cell Metab. 2018;28(2):282-8.e3.
38. Zoico E, Darra E, Rizzatti V, Budui S, Franceschetti G, Mazzali G, et al. Adipocytes WNT5a mediated dedifferentiation: a possible target in pancreatic cancer microenvironment. Oncotarget. 2016;7(15):20223-35.
39. Lutz TA, Woods SC. Overview of animal models of obesity. Current protocols in pharmacology. 2012;Chapter 5:Unit5.61-Unit5.
40. Vaughan KL, Mattison JA. Obesity and Aging in Humans and Nonhuman Primates: A Mini-Review. Gerontology. 2016;62(6):611-7.

41. National Research Council Committee on D. The National Academies Collection: Reports funded by National Institutes of Health. Laboratory Animal Management: Dogs. Washington (DC): National Academies Press (US)

Copyright 1994 by the National Academy of Sciences. All rights reserved.; 1994.
42. Davidson MK, Lindsey JR, Davis JK. Requirements and selection of an animal model. Israel journal of medical sciences. 1987;23(6):551-5.
43. Jackson SJ, Andrews N, Ball D, Bellantuono I, Gray J, Hachoumi L, et al. Does age matter? The impact of rodent age on study outcomes. Lab Anim. 2017;51(2):160-9.
44. Flurkey K CJ, Harrison DE. The mouse in biomedical research. 2nd ed. Burlington: Academic Press2007.
45. Furuhashi M, Saitoh S, Shimamoto K, Miura T. Fatty Acid-Binding Protein 4 (FABP4): Pathophysiological Insights and Potent Clinical Biomarker of Metabolic and Cardiovascular Diseases. Clin Med Insights Cardiol. 2015;8(Suppl 3):23-33.
46. Mead JR, Irvine SA, Ramji DP. Lipoprotein lipase: structure, function, regulation, and role in disease. Journal of molecular medicine (Berlin, Germany). 2002;80(12):753-69.
47. Zhang S, Liu G, Xu C, Liu L, Zhang Q, Xu Q, et al. Perilipin 1 Mediates Lipid Metabolism Homeostasis and Inhibits Inflammatory Cytokine Synthesis in Bovine Adipocytes. Frontiers in immunology. 2018;9:467-.
48. Zechner R, Zimmermann R, Eichmann TO, Kohlwein SD, Haemmerle G, Lass A, et al. FAT SIGNALS--lipases and lipolysis in lipid metabolism and signaling. Cell metabolism. 2012;15(3):279-91.
49. Conde J, Scotece M, Gomez R, Lopez V, Gomez-Reino JJ, Lago F, et al. Adipokines: biofactors from white adipose tissue. A complex hub among inflammation, metabolism, and immunity. BioFactors (Oxford, England). 2011;37(6):413-20.
50. Lehr S, Hartwig S, Sell H. Adipokines: a treasure trove for the discovery of biomarkers for metabolic disorders. Proteomics Clinical applications. 2012;6(1-2):91-101.
51. Wang ZV, Scherer PE. Adiponectin, the past two decades. Journal of Molecular Cell Biology. 2016;8(2):93-100.
52. Lee M-H, Klein RL, El-Shewy HM, Luttrell DK, Luttrell LM. The adiponectin receptors AdipoR1 and AdipoR2 activate ERK1/2 through a Src/Ras-dependent pathway and stimulate cell growth. Biochemistry. 2008;47(44):11682-92.
53. Kadowaki T, Yamauchi T. Adiponectin and adiponectin receptors. Endocrine reviews. 2005;26(3):439-51.
54. Stefan N, Stumvoll M. Adiponectin - Its Role in Metabolism and Beyond. Hormone and metabolic research = Hormon- und Stoffwechselforschung = Hormones et metabolisme. 2002;34(09):469-74.
55. Heiker John T, Kosel D, Beck-Sickinger Annette G. Molecular mechanisms of signal transduction via adiponectin and adiponectin receptors. Biological Chemistry2010. p. 1005.
56. Yamauchi T, Kamon J, Minokoshi Y, Ito Y, Waki H, Uchida S, et al. Adiponectin stimulates glucose utilization and fatty-acid oxidation by activating AMP-activated protein kinase. Nature medicine. 2002;8(11):1288-95.
57. Yamauchi T, Kamon J, Waki H, Terauchi Y, Kubota N, Hara K, et al. The fat-derived hormone adiponectin reverses insulin resistance associated with both lipoatrophy and obesity. Nature medicine. 2001;7(8):941-6.
58. Berg AH, Combs TP, Du X, Brownlee M, Scherer PE. The adipocyte-secreted protein Acrp30 enhances hepatic insulin action. Nature medicine. 2001;7(8):947-53.

59. Pajvani UB, Du X, Combs TP, Berg AH, Rajala MW, Schulthess T, et al. Structure-function studies of the adipocyte-secreted hormone Acrp30/adiponectin. Implications fpr metabolic regulation and bioactivity. The Journal of biological chemistry. 2003;278(11):9073-85.
60. Gorska E, Popko K, Stelmaszczyk-Emmel A, Ciepiela O, Kucharska A, Wasik M. Leptin receptors. Eur J Med Res. 2010;15 Suppl 2(Suppl 2):50-4.
61. Boden G, Chen X, Mozzoli M, Ryan I. Effect of fasting on serum leptin in normal human subjects. The Journal of clinical endocrinology and metabolism. 1996;81(9):3419-23.
62. Chan JL, Heist K, DePaoli AM, Veldhuis JD, Mantzoros CS. The role of falling leptin levels in the neuroendocrine and metabolic adaptation to short-term starvation in healthy men. The Journal of clinical investigation. 2003;111(9):1409-21.
63. Chan JL, Mantzoros CS. Role of leptin in energy-deprivation states: normal human physiology and clinical implications for hypothalamic amenorrhoea and anorexia nervosa. Lancet. 2005;366(9479):74-85.
64. Kelesidis T, Kelesidis I, Chou S, Mantzoros CS. Narrative review: the role of leptin in human physiology: emerging clinical applications. Annals of internal medicine. 2010;152(2):93-100.
65. Licinio J, Mantzoros C, Negrao AB, Cizza G, Wong ML, Bongiorno PB, et al. Human leptin levels are pulsatile and inversely related to pituitary-adrenal function. Nature medicine. 1997;3(5):575-9.
66. Sinha MK, Ohannesian JP, Heiman ML, Kriauciunas A, Stephens TW, Magosin S, et al. Nocturnal rise of leptin in lean, obese, and non-insulin-dependent diabetes mellitus subjects. The Journal of clinical investigation. 1996;97(5):1344-7.
67. Kar A, Gutierrez-Hartmann A. Molecular mechanisms of ETS transcription factor-mediated tumorigenesis. Crit Rev Biochem Mol Biol. 2013;48(6):522-43.
68. Gutierrez-Hartmann A, Duval DL, Bradford AP. ETS transcription factors in endocrine systems. Trends in Endocrinology & Metabolism. 2007;18(4):150-8.
69. Birsoy K, Berry R, Wang T, Ceyhan O, Tavazoie S, Friedman JM, et al. Analysis of gene networks in white adipose tissue development reveals a role for ETS2 in adipogenesis. Development. 2011;138(21):4709.
70. He Q, Gao Z, Yin J, Zhang J, Yun Z, Ye J. Regulation of HIF-1{alpha} activity in adipose tissue by obesity-associated factors: adipogenesis, insulin, and hypoxia. American journal of physiology Endocrinology and metabolism. 2011;300(5):E877-E85.
71. Liu T, Zhang L, Joo D, Sun S-C. NF-κB signaling in inflammation. Signal transduction and targeted therapy. 2017;2:17023.
72. Sun SC, Chang JH, Jin J. Regulation of nuclear factor-kappaB in autoimmunity. Trends in immunology. 2013;34(6):282-9.
73. Karin M, Delhase M. The I kappa B kinase (IKK) and NF-kappa B: key elements of proinflammatory signalling. Seminars in immunology. 2000;12(1):85-98.
74. Xiao G, Harhaj EW, Sun SC. NF-kappaB-inducing kinase regulates the processing of NF-kappaB2 p100. Molecular cell. 2001;7(2):401-9.
75. Senftleben U, Cao Y, Xiao G, Greten FR, Krahn G, Bonizzi G, et al. Activation by IKKalpha of a second, evolutionary conserved, NF-kappa B signaling pathway. Science (New York, NY). 2001;293(5534):1495-9.
76. Lee MJ. Transforming growth factor beta superfamily regulation of adipose tissue biology in obesity. Biochimica et biophysica acta Molecular basis of disease. 2018;1864(4 Pt A):1160-71.

77. Clark DA, Coker R. Transforming growth factor-beta (TGF-beta). The international journal of biochemistry & cell biology. 1998;30(3):293-8.
78. Sporn M, Roberts A, Wakefield L, Assoian R. Transforming growth factor-beta: biological function and chemical structure. Science (New York, NY). 1986;233(4763):532-4.
79. Chin D, Boyle GM, Parsons PG, Coman WB. What is transforming growth factor-beta (TGF-β)? British Journal of Plastic Surgery. 2004;57(3):215-21.
80. Verrecchia F, Mauviel A. Transforming growth factor-beta and fibrosis. World J Gastroenterol. 2007;13(22):3056-62.
81. Gilboa L, Wells RG, Lodish HF, Henis YI. Oligomeric structure of type I and type II transforming growth factor beta receptors: homodimers form in the ER and persist at the plasma membrane. The Journal of cell biology. 1998;140(4):767-77.
82. Xu H, Barnes GT, Yang Q, Tan G, Yang D, Chou CJ, et al. Chronic inflammation in fat plays a crucial role in the development of obesity-related insulin resistance. The Journal of clinical investigation. 2003;112(12):1821-30.
83. Datta R, Podolsky MJ, Atabai K. Fat fibrosis: friend or foe? JCI insight. 2018;3(19).
84. Bolinder J, Kerckhoffs DA, Moberg E, Hagstrom-Toft E, Arner P. Rates of skeletal muscle and adipose tissue glycerol release in nonobese and obese subjects. Diabetes. 2000;49(5):797-802.
85. Hoeben A, Landuyt B, Highley MS, Wildiers H, Van Oosterom AT, De Bruijn EA. Vascular endothelial growth factor and angiogenesis. Pharmacological reviews. 2004;56(4):549-80.
86. Buechler C, Krautbauer S, Eisinger K. Adipose tissue fibrosis. World journal of diabetes. 2015;6(4):548-53.
87. Yun Z, Maecker HL, Johnson RS, Giaccia AJ. Inhibition of PPAR gamma 2 gene expression by the HIF-1-regulated gene DEC1/Stra13: a mechanism for regulation of adipogenesis by hypoxia. Developmental cell. 2002;2(3):331-41.
88. Engin A. Adipose Tissue Hypoxia in Obesity and Its Impact on Preadipocytes and Macrophages: Hypoxia Hypothesis. Advances in experimental medicine and biology. 2017;960:305-26.
89. Greijer AE, van der Wall E. The role of hypoxia inducible factor 1 (HIF-1) in hypoxia induced apoptosis. Journal of clinical pathology. 2004;57(10):1009-14.
90. Yin J, Gao Z, He Q, Zhou D, Guo Z, Ye J. Role of hypoxia in obesity-induced disorders of glucose and lipid metabolism in adipose tissue. American journal of physiology Endocrinology and metabolism. 2009;296(2):E333-E42.
91. Italiani P, Boraschi D. From Monocytes to M1/M2 Macrophages: Phenotypical vs. Functional Differentiation. Frontiers in immunology. 2014;5:514-.
92. D'Ignazio L, Rocha S. Hypoxia Induced NF-κB. Cells. 2016;5(1):10.
93. Chung KJ, Nati M, Chavakis T, Chatzigeorgiou A. Innate immune cells in the adipose tissue. Reviews in endocrine & metabolic disorders. 2018;19(4):283-92.
94. Ferrante AW, Jr. The immune cells in adipose tissue. Diabetes, obesity & metabolism. 2013;15 Suppl 3:34-8.
95. Hill AA, Reid Bolus W, Hasty AH. A decade of progress in adipose tissue macrophage biology. Immunological reviews. 2014;262(1):134-52.
96. Milos M, Martin H. The role of adipose tissue immune cells in obesity and low-grade inflammation. Journal of Endocrinology. 2014;222(3):R113-R27.
97. Lumeng CN, Maillard I, Saltiel AR. T-ing up inflammation in fat. Nature medicine. 2009;15(8):846-7.

98. Li C, Xu MM, Wang K, Adler AJ, Vella AT, Zhou B. Macrophage polarization and meta-inflammation. Translational Research. 2018;191:29-44.
99. Lumeng CN, Bodzin JL, Saltiel AR. Obesity induces a phenotypic switch in adipose tissue macrophage polarization. The Journal of clinical investigation. 2007;117(1):175-84.
100. Zeyda M, Stulnig TM. Adipose tissue macrophages. Immunology letters. 2007;112(2):61-7.
101. Ryan VH, German AJ, Wood IS, Hunter L, Morris P, Trayhurn P. Adipokine expression and secretion by canine adipocytes: stimulation of inflammatory adipokine production by LPS and TNFalpha. Pflugers Archiv : European journal of physiology. 2010;460(3):603-16.
102. Feuerer M, Herrero L, Cipolletta D, Naaz A, Wong J, Nayer A, et al. Lean, but not obese, fat is enriched for a unique population of regulatory T cells that affect metabolic parameters. Nature medicine. 2009;15(8):930-9.
103. Nishimura S, Manabe I, Nagasaki M, Eto K, Yamashita H, Ohsugi M, et al. CD8+ effector T cells contribute to macrophage recruitment and adipose tissue inflammation in obesity. Nature medicine. 2009;15(8):914-20.
104. Winer S, Chan Y, Paltser G, Truong D, Tsui H, Bahrami J, et al. Normalization of obesity-associated insulin resistance through immunotherapy. Nature medicine. 2009;15(8):921-9.
105. Morin SO, Poggi M, Alessi MC, Landrier JF, Nunes JA. Modulation of T Cell Activation in Obesity. Antioxidants & redox signaling. 2017;26(10):489-500.
106. Nam H, Ferguson BS, Stephens JM, Morrison RF. Impact of obesity on IL-12 family gene expression in insulin responsive tissues. Biochimica et Biophysica Acta (BBA) - Molecular Basis of Disease. 2013;1832(1):11-9.
107. Dalmas E, Venteclef N, Caer C, Poitou C, Cremer I, Aron-Wisnewsky J, et al. T cell-derived IL-22 amplifies IL-1beta-driven inflammation in human adipose tissue: relevance to obesity and type 2 diabetes. Diabetes. 2014;63(6):1966-77.
108. Fabbrini E, Cella M, McCartney SA, Fuchs A, Abumrad NA, Pietka TA, et al. Association between specific adipose tissue CD4+ T-cell populations and insulin resistance in obese individuals. Gastroenterology. 2013;145(2):366-74.e1-3.
109. Winer DA, Winer S, Chng MHY, Shen L, Engleman EG. B Lymphocytes in obesity-related adipose tissue inflammation and insulin resistance. Cell Mol Life Sci. 2014;71(6):1033-43.
110. Frasca D, Blomberg BB. Adipose Tissue Inflammation Induces B Cell Inflammation and Decreases B Cell Function in Aging. Frontiers in immunology. 2017;8:1003-.
111. Kunisawa J, Kurashima Y, Gohda M, Higuchi M, Ishikawa I, Miura F, et al. Sphingosine 1-phosphate regulates peritoneal B-cell trafficking for subsequent intestinal IgA production. Blood. 2007;109(9):3749-56.
112. Martin F, Kearney JF. B1 cells: similarities and differences with other B cell subsets. Current opinion in immunology. 2001;13(2):195-201.
113. Lund FE. Cytokine-producing B lymphocytes-key regulators of immunity. Current opinion in immunology. 2008;20(3):332-8.
114. Yanaba K, Bouaziz JD, Haas KM, Poe JC, Fujimoto M, Tedder TF. A regulatory B cell subset with a unique CD1dhiCD5+ phenotype controls T cell-dependent inflammatory responses. Immunity. 2008;28(5):639-50.
115. Mauri C, Ehrenstein MR. The 'short' history of regulatory B cells. Trends in immunology. 2008;29(1):34-40.

116. Weisberg SP, McCann D, Desai M, Rosenbaum M, Leibel RL, Ferrante AW, Jr. Obesity is associated with macrophage accumulation in adipose tissue. The Journal of clinical investigation. 2003;112(12):1796-808.
117. Strissel KJ, DeFuria J, Shaul ME, Bennett G, Greenberg AS, Obin MS. T-cell recruitment and Th1 polarization in adipose tissue during diet-induced obesity in C57BL/6 mice. Obesity (Silver Spring, Md). 2010;18(10):1918-25.
118. Meng X-M, Nikolic-Paterson DJ, Lan HY. Inflammatory processes in renal fibrosis. Nature Reviews Nephrology. 2014;10:493.
119. Sibley CD, Parkins MD, Rabin HR, Duan K, Norgaard JC, Surette MG. A polymicrobial perspective of pulmonary infections exposes an enigmatic pathogen in cystic fibrosis patients. Proceedings of the National Academy of Sciences. 2008;105(39):15070.
120. Yan C, Li B, Fan F, Du Y, Ma R, Cheng X-D, et al. The roles of Toll-like receptor 4 in the pathogenesis of pathogen-associated biliary fibrosis caused by Clonorchis sinensis. Scientific reports. 2017;7(1):3909-.
121. Sun K, Tordjman J, Clément K, Scherer Philipp E. Fibrosis and Adipose Tissue Dysfunction. Cell Metabolism. 2013;18(4):470-7.
122. Walker RW, Allayee H, Inserra A, Fruhwirth R, Alisi A, Devito R, et al. Macrophages and fibrosis in adipose tissue are linked to liver damage and metabolic risk in obese children. Obesity (Silver Spring, Md). 2014;22(6):1512-9.
123. Ectopic Fat and Insulin Resistance: Pathophysiology and Effect of Diet and Lifestyle Interventions. International Journal of Endocrinology. 2012;2012:18.
124. Abdennour M, Reggio S, Le Naour G, Liu Y, Poitou C, Aron-Wisnewsky J, et al. Association of Adipose Tissue and Liver Fibrosis With Tissue Stiffness in Morbid Obesity: Links With Diabetes and BMI Loss After Gastric Bypass. The Journal of Clinical Endocrinology & Metabolism. 2014;99(3):898-907.
125. Divoux A, Clément K. Architecture and the extracellular matrix: the still unappreciated components of the adipose tissue. Obesity Reviews. 2011;12(5):e494-e503.
126. Bornstein P, Sage EH. Matricellular proteins: extracellular modulators of cell function. Current opinion in cell biology. 2002;14(5):608-16.
127. Dobin A, Davis CA, Schlesinger F, Drenkow J, Zaleski C, Jha S, et al. STAR: ultrafast universal RNA-seq aligner. Bioinformatics (Oxford, England). 2013;29(1):15-21.
128. Li H, Handsaker B, Wysoker A, Fennell T, Ruan J, Homer N, et al. The Sequence Alignment/Map format and SAMtools. Bioinformatics (Oxford, England). 2009;25(16):2078-9.
129. Madsen JGS, Schmidt SF, Larsen BD, Loft A, Nielsen R, Mandrup S. iRNA-seq: computational method for genome-wide assessment of acute transcriptional regulation from total RNA-seq data. Nucleic Acids Res. 2015;43(6):e40-e.
130. Love MI, Huber W, Anders S. Moderated estimation of fold change and dispersion for RNA-seq data with DESeq2. Genome Biology. 2014;15(12):550.
131. Kolde R. pheatmap: Pretty Heatmaps. 2019.
132. Yu G, Wang L-G, Han Y, He Q-Y. clusterProfiler: an R package for comparing biological themes among gene clusters. OMICS. 2012;16(5):284-7.
133. Slenter DN, Kutmon M, Hanspers K, Riutta A, Windsor J, Nunes N, et al. WikiPathways: a multifaceted pathway database bridging metabolomics to other omics research. Nucleic Acids Res. 2018;46(D1):D661-d7.
134. Balwierz PJ, Pachkov M, Arnold P, Gruber AJ, Zavolan M, van Nimwegen E. ISMARA: automated modeling of genomic signals as a democracy of regulatory motifs. Genome research. 2014;24(5):869-84.

135. Pellegrinelli V, Carobbio S, Vidal-Puig A. Adipose tissue plasticity: how fat depots respond differently to pathophysiological cues. Diabetologia. 2016;59(6):1075-88.
136. Gawronska-Kozak B, Staszkiewicz J, Gimble JM, Kirk-Ballard H. Recruitment of fat cell precursors during high fat diet in C57BL/6J mice is fat depot specific. Obesity (Silver Spring, Md). 2014;22(4):1091-102.
137. Slenter DN, Kutmon M, Hanspers K, Riutta A, Windsor J, Nunes N, et al. WikiPathways: a multifaceted pathway database bridging metabolomics to other omics research. Nucleic Acids Res. 2017;46(D1):D661-D7.
138. Kanehisa M, Goto S. KEGG: kyoto encyclopedia of genes and genomes. Nucleic Acids Res. 2000;28(1):27-30.
139. Benjamini Y, Hochberg Y. Controlling the False Discovery Rate: A Practical and Powerful Approach to Multiple Testing. Journal of the Royal Statistical Society Series B (Methodological). 1995;57(1):289-300.
140. Queipo-Ortuño MI, Escoté X, Ceperuelo-Mallafré V, Garrido-Sanchez L, Miranda M, Clemente-Postigo M, et al. FABP4 dynamics in obesity: discrepancies in adipose tissue and liver expression regarding circulating plasma levels. PloS one. 2012;7(11):e48605-e.
141. Kandasamy K, Mohan SS, Raju R, Keerthikumar S, Kumar GS, Venugopal AK, et al. NetPath: a public resource of curated signal transduction pathways. Genome Biol. 2010;11(1):R3.
142. Madsen JGS, Rauch A, Van Hauwaert EL, Schmidt SF, Winnefeld M, Mandrup S. Integrated analysis of motif activity and gene expression changes of transcription factors. Genome research. 2018;28(2):243-55.